17. SITE 941[1]

Shipboard Scientific Party[2]

HOLE 941A

Date occupied: 6 May 1994

Date departed: 7 May 1994

Time on hole: 1 day, 21 hr, 30 min

Position: 5°22.384′N, 48°1.723′W

Bottom felt (drill pipe measurement from rig floor, m): 3392.2

Distance between rig floor and sea level (m): 11.30

Water depth (drill pipe measurement from sea level, m): 3380.9

Penetration (m): 177.90

Number of cores (including cores having no recovery): 19

Total length of cored section (m): 177.66

Total core recovered (m): 122.85

Core recovery (%): 69

Oldest sediment cored:
Depth (mbsf): 177.90
Nature: Silty clay
Earliest age: Pleistocene

HOLE 941B

Date occupied: 7 May 1994

Date departed: 8 May 1994

Time on hole: 22 hr, 15 min

Position: 5°22.110′N, 48°1.610′W

Bottom felt (drill pipe measurement from rig floor, m): 3388.8

Distance between rig floor and sea level (m): 11.30

Water depth (drill pipe measurement from sea level, m): 3377.5

Penetration (m): 85.10

Number of cores (including cores having no recovery): 12

Total length of cored section (m): 85.10

Total core recovered (m): 96.15

Core recovery (%): 113

Oldest sediment cored:
Depth (mbsf): 85.10
Nature: Silty clay
Earliest age: Pleistocene

Principal results: Site 941 (proposed Site AF-5) is located on the western side of the Amazon Fan in a surficial debris-flow deposit that fills a depression between two levees. The site was intended to determine the lithologic nature and geotechnical properties of the debris-flow deposit for an understanding of debris-flow dynamics and for comparison to deeply buried debris-flow deposits recovered at Sites 931, 933, 935, and 936. It was also intended to date the underlying levee flank deposits that may be related to the Purple Channel-levee System.

The site was selected from a *Ewing* seismic profile (E9209; 2325UTC on 21 Sept. 1993). The site was confirmed by a short seismic survey from the *JOIDES Resolution*.

Hole 941A was cored by APC to 62.3 mbsf, then by XCB to 177.9 mbsf, with total hole recovery of 122.85 m (69.1%). An attempt was then made to log the hole using the Quad-combo and FMS tools from 175 to 90 mbsf, but the hole kept closing, so logging was abandoned. Hole 941B was offset 500 m south-southeast of Hole 941A to assess the lateral extent of large blocks in the debris-flow deposit. Hole 941B was cored by recovery using the APC tool until the sediment became too consolidated at 85.1 mbsf, and 96.15 m was recovered (113%, the extra sediment largely as a result of flow-in). Whole-round samples for geotechnical analysis were taken in Hole 941B.

One temperature measurement was made at 53 mbsf (ADARA) and, together with the mud-line temperature, shows a mean geothermal gradient of 32°C/km. There was gas expansion in many cores, but less than was experienced at most other sites during Leg 155. Methane was found throughout the hole, but higher hydrocarbons were not detected. Extreme gas expansion and a honeycomb structure to the mud were observed at 45 mbsf in Hole 941B.

Four lithologic units are recognized, using Hole 941A as a type section:

Unit I (0–0.98 mbsf) is a Holocene bioturbated nannofossil-foraminifer clay, with about 30% carbonate, similar to Unit I at previous Leg 155 sites. Hole 941A is exceptional in that the calcareous clay is underlain by a foraminifer sand (80% carbonate) with common pteropods, interpreted as a turbidite. This sand is absent in Hole 941B.

Unit II (0.98–5.30 mbsf) consists of dark gray mud, with carbonate content between 0.6% and 5.7%. Euhedral crystals of ikaite, several centimeters in size, were found at 3–4 mbsf. They began to disintegrate a few hours after the core was split.

Unit III (5.30–129.70 mbsf) consists of mud and sandy mud of varying consistency and color that shows soft-sediment deformation. The presence of clasts is indicated by abrupt changes in lithology and color. Folds are present on scales from centimeters to meters. Some boundaries between clasts show shear deformation. Fault contacts are common, and layering in many clasts is offset by a series of microfaults. Rare pebbles of siltstone and unidentified rock are found, but sand is sparse. In general, the unit appears to be a clast-supported breccia, and little matrix mud was identified. The unit is interpreted as a debris-flow or slump deposit, but the number of depositional events is uncertain. Recovery was very poor in the lower half of this unit (24% from 72 to 130 mbsf).

Unit IV (129.70–177.90 mbsf) consists of mud with many laminae and thin beds of silt and fine sand, similar to levee sequences cored at other sites during Leg 155.

Total organic carbon is lower than at other Leg 155 sites, and is typically 0.6%–0.85%. Nevertheless, measured headspace methane concentrations are similar to those at other sites.

As at other Leg 155 sites, Unit I is Holocene in age. Unit II also contains a Holocene foraminiferal fauna including *G. tumida*. Unit IV contains a Y-zone fauna lacking *P. obliquiloculata* and is therefore interpreted as younger than 40 ka. The age of Unit IV supports the suggestion that the levee correlates with the Purple Channel-levee System.

[1]Flood, R.D., Piper, D.J.W., Klaus, A., et al., 1995. *Proc. ODP, Init. Repts.*, 155: College Station, TX (Ocean Drilling Program).

[2]Shipboard Scientific Party is as given in the list of participants in the contents.

Clasts in the debris-flow deposit are of two main biozones. One type comprises Y zone assemblages, including *P. obliquiloculata* (i.e., probably 40–85 ka). The other consists of X zone assemblages, including a relatively high abundance of *G. menardii, G. tumida,* and *G. tumida flexuosa,* indicating an interglacial assemblage probably from isotopic Stage 5. Preliminary data suggest that biozones alternate down through the debris-flow deposit, with each zone being 10–20 m thick. In addition, clasts of olive-gray mud with 7% total carbonate at 30–35 mbsf contain rich Miocene nannoflora. Echinoid plates are locally abundant. Bathyal benthic foraminifers, pteropods, ostracod shells, and fish scales are found also in Unit III.

Unlike at previous Sites 931, 933, 935, and 936, where deeply buried debris-flow deposits were cored, there is no decrease in wet-bulk density and increase in porosity in the levee sediment immediately underlying the debris flow, nor is there evidence for overpressuring.

A pore-water sample at 112 mbsf has a salinity of 29.5 and unusually low chloride (496 mM) and magnesium (29.5 mM). These low concentrations suggest pore-water dilution, probably through melting of gas hydrates. The extreme gas expansion and honeycomb structure at 45 mbsf may also be evidence of gas hydrates.

This site provided a detailed section through a young debris-flow deposit, which appears to be of earliest Holocene age. It shows many of the sedimentological features of more deeply buried debris-flow deposits. The general lack of muddy matrix material is noteworthy. Blocks are inferred to range in size from centimeters to many meters and are both folded and faulted. The repetitive biozones suggest that the debris-flow deposit may have formed by repeated retrogressive failure of last glacial sediment overlying last interglacial sediment. Previous seismic-reflection profiles and confirmation of acoustic facies by Leg 155 holes has shown that about 20% of the sediment in the upper few hundred meters of the Amazon Fan is made up of a few vast debris-flow deposits of the type cored at this site.

SETTING AND OBJECTIVES

Introduction

Site 941 (proposed Site AF-5) is located in a surficial debris-flow deposit that fills a depression between two levees on the western side of the Amazon Fan. This debris-flow deposit may be a sedimentological analogue of debris-flow deposits sampled deeper in the section at Sites 931, 933, 935, and 936 (e.g., Unit R and/or smaller debris-flow deposits). Holes at Site 941 penetrate through the debris flow into the flank of a channel-levee system that may be related to the Purple Channel-levee System.

Setting

Site 941 is located on the Western Debris Flow, where one or more debris-flow deposits have filled in the depression between two levees (Fig. 1; Damuth and Embley, 1981; Damuth et al., 1988). The debris-flow deposit has a maximum thickness of 200 ms (approximately 155 m) along the seismic line on which the site is located, and is 165 ms (approximately 125 m) thick at Site 941 (Fig. 2). The surface of the debris-flow deposit in this area appears blocky with a local relief of about 5 m (Fig. 3); however, a 5-ms-thick (4 m) laminated layer covers the debris-flow deposit. A nearby piston core (V18-20; 5°58.2′N, 48°22.8′W; Damuth and Embley, 1981) from this debris-flow deposit shows an undisturbed layer 4.85 m thick overlying deformed beds. Overall this debris-flow deposit has a nearly flat upper surface that rises only slightly above the level of the confining levees (Fig. 2). GLORIA side-scan sonar images show a highly reflective zone in the region between the buried levee crests, consistent with a deformed interval near the surface (Damuth et al., 1988). Downslope from Site 941, a 3.5-kHz profile shows that the debris-flow surface becomes first blocky and then acoustically transparent before terminating abruptly 38 km from Site 941 (Fig. 4).

The site was selected from a *Ewing* seismic profile (E9209; 2325UTC on 21 Sept. 1993; Fig. 2) and was chosen to sample the debris-flow deposit(s) where they are thick, but also to penetrate into the flank of the underlying levee. This position is equivalent to 0937UTC on a *Farnella* seismic line on 15 Jan. 1982, and to our *JOIDES Resolution* seismic line at 0228UTC on 6 May 1994.

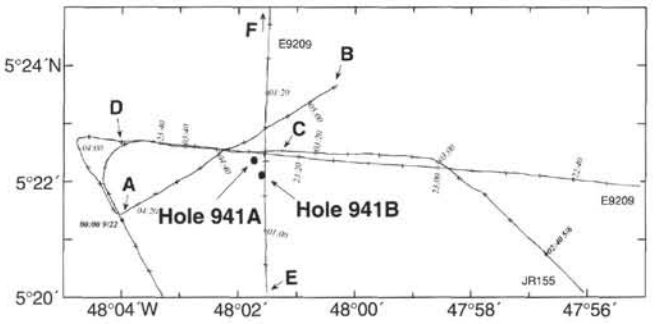

Figure 1. Location of Site 941 showing *Ewing* (E9209) and *JOIDES Resolution* (JR155) ship tracks on which Site 941 is located. A–B is the seismic profile in Figure 2; C–D and E–F are the 3.5-kHz profiles in Figures 3 and 4, respectively.

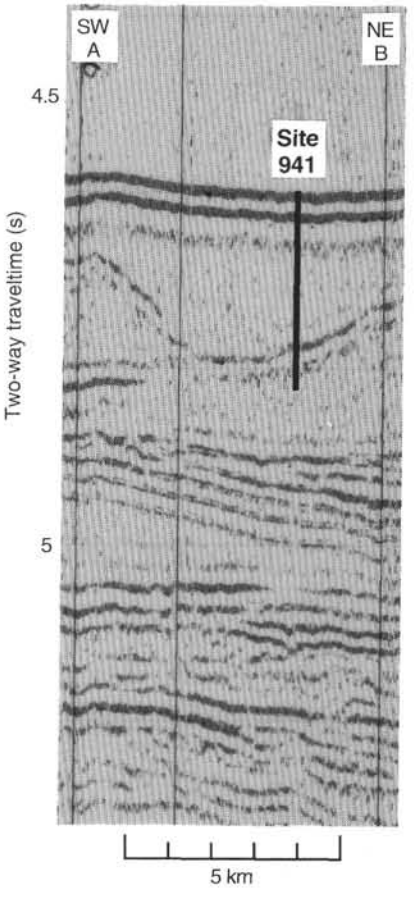

Figure 2. Seismic profile (*JOIDES Resolution,* 6 May, 0415–0505) through Site 941 (A–B in Fig. 1).

Objectives

The principal objectives at Site 941 were:

1. To determine the nature of debris-flow deposits at this site for an understanding of debris-flow dynamics and for comparison to deeply buried debris-flow deposits recovered at a number of sites during this leg.

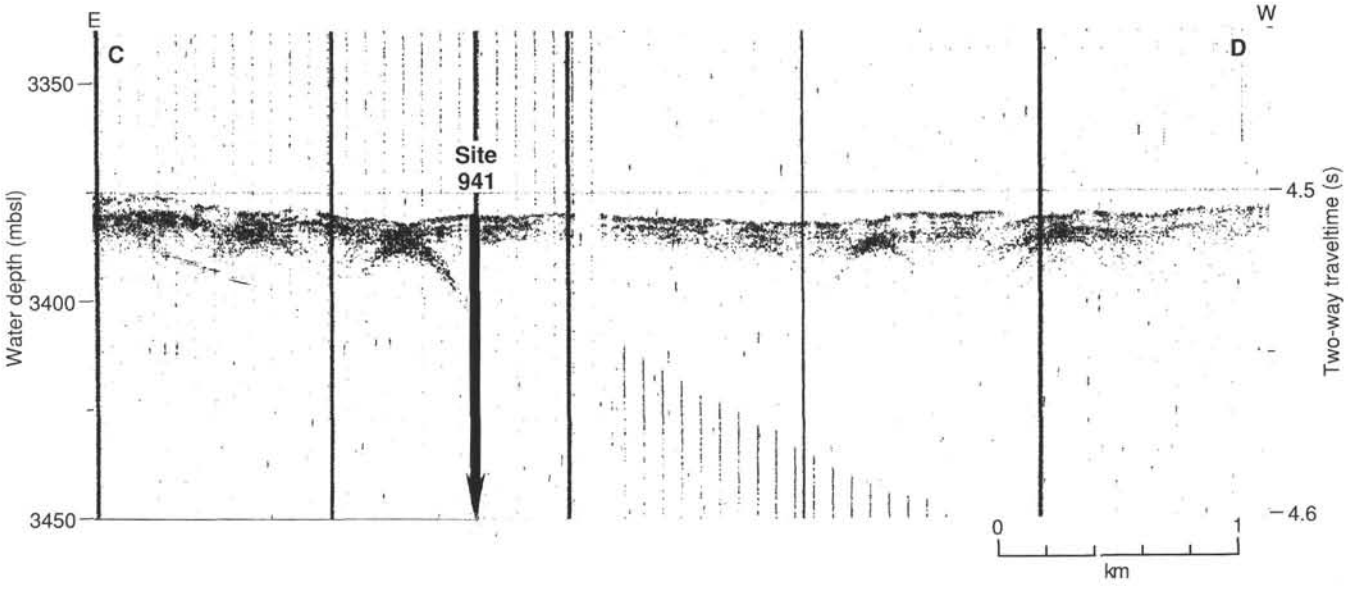

Figure 3. A 3.5-kHz profile through Site 941 (C–D in Fig. 1).

2. To determine whether there is more than one debris-flow deposit and, if possible, to characterize their sources and ages.
3. To obtain high-quality samples of debris-flow material and related sediment for geotechnical testing.
4. To characterize the sediment of the buried channel-levee system and, if possible, date the deposit.

OPERATIONS

Transit: Site 940 to Site 941 (AF-5)

The 29.4-nmi transit from Site 940 to Site 941 (AF-5) took 2.7 hr. We conducted a 16.7-nmi seismic survey to confirm the proposed position based on pre-cruise data. At 0220 hr 6 May, we deployed a beacon at 5°22.51′N, 48°1.60′W. Surface currents were estimated to range from 0.5 to 1.65 kt from the northeast, but the beacon was carried 600 m to the southeast by deeper currents before landing on the seafloor.

Hole 941A

We positioned the ship 300 m to the northwest of the beacon, positioned the bit at 3388.0 mbrf, and spudded Hole 941A at 0942 hr 6 May. We assembled a BHA similar to that used at Site 939. The distance from sea level to rig floor, which depends on the ship's draft, was 11.35 m for Holes 941A and 941B. Core 1H recovered 5.30 m, and the mud line was defined to be at 3392.2 mbrf. Cores 1H through 7H were taken from 3392.2 to 3454.5 mbrf (0–62.3 mbsf) and recovered 62.12 m (99.7%). Cores 3H through 7H were oriented using the Tensor tool, and an ADARA heat-flow measurement was made during Core 6H. Parts of Cores 3H, 5H, 6H, 7H, and 16X were disturbed as a result of either gas-induced extrusion of core from the liner onto

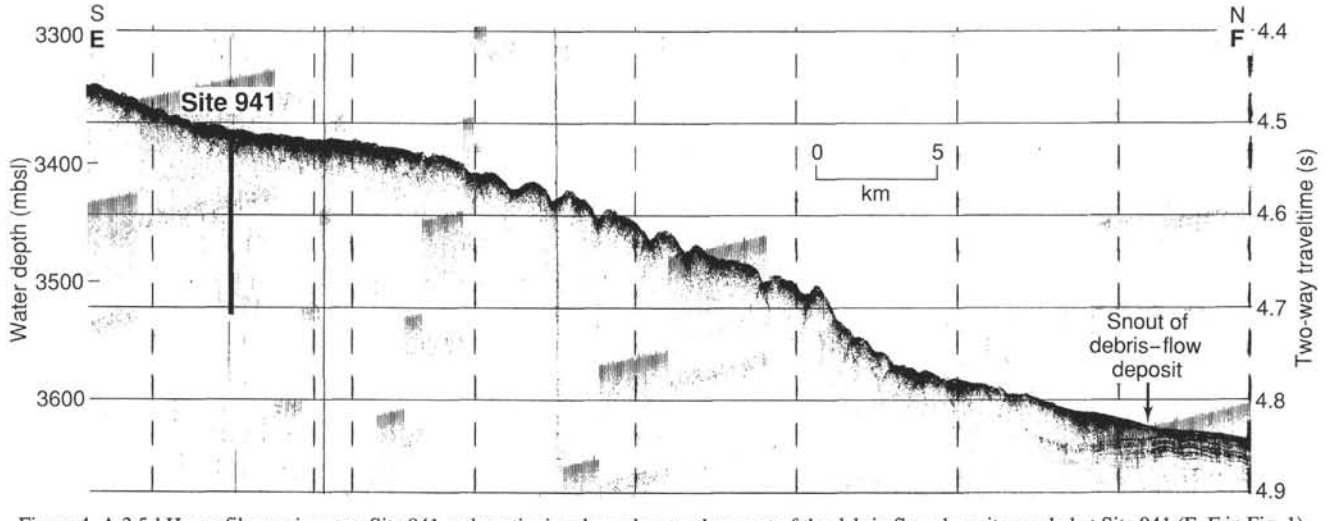

Figure 4. A 3.5-kHz profile passing near Site 941 and continuing downslope to the snout of the debris-flow deposit sampled at Site 941 (E–F in Fig. 1).

Table 1. Site 941 coring summary.

Core	Date (1994)	Time (UTC)	Depth (mbsf)	Length cored (m)	Length recovered (m)	Recovery (%)
155-941A-						
1H	May 6	1355	0.0–5.3	5.3	5.30	100.0
2H	May 6	1450	5.3–14.8	9.5	9.95	105.0
3H	May 6	1545	14.8–24.3	9.5	10.05	105.8
4H	May 6	1645	24.3–33.8	9.5	9.87	104.0
5H	May 6	1730	33.8–43.3	9.5	8.77	92.3
6H	May 6	1845	43.3–52.8	9.5	10.43	109.8
7H	May 6	1930	52.8–62.3	9.5	7.85	82.6
8X	May 6	2150	62.3–71.8	9.5	3.98	41.9
9X	May 6	2300	71.8–81.3	9.5	3.03	31.9
10X	May 6	2355	81.3–90.8	9.5	1.71	18.0
12X	May 7	0310	100.7–110.3	9.6	0.00	0.0
13X	May 7	0505	110.3–120.0	9.7	5.09	52.5
14X	May 7	0720	120.0–129.7	9.7	4.08	42.0
15X	May 7	0840	129.7–139.3	9.6	9.76	101.0
16X	May 7	1000	139.3–148.9	9.6	8.52	88.7
17X	May 7	1120	148.9–158.4	9.5	7.57	80.0
18X	May 7	1255	158.6–168.2	9.6	9.08	94.6
19X	May 7	1430	168.2–177.9	9.7	7.63	78.6
Coring totals				177.7	122.9	69.0
155-941B-						
1H	May 8	0550	0.0–6.6	6.6	6.60	100.0
2H	May 8	0650	6.6–16.1	9.5	10.21	107.5
3H	May 8	0745	16.1–25.6	9.5	10.00	105.2
4H	May 8	0845	25.6–35.1	9.5	9.89	104.0
5H	May 8	0940	35.1–44.6	9.5	9.42	99.1
6H	May 8	1145	44.6–49.6	5.0	7.91	158.0
7H	May 8	1300	49.6–59.1	9.5	10.23	107.7
8H	May 8	1410	59.1–64.1	5.0	6.95	139.0
9H	May 8	1525	64.1–70.1	6.0	5.58	93.0
10H	May 8	1625	70.1–75.1	5.0	5.62	112.0
11H	May 8	1715	75.1–80.1	5.0	7.13	142.0
12H	May 8	1850	80.1–85.1	5.0	6.61	132.0
Coring totals				85.1	96.2	113.00

Note: An expanded version of this coring summary table that includes lengths and depths of sections, location of whole-round samples, and comments on sampling disturbance is included on the CD-ROM in the back pocket of this volume.

the rig floor or collapsed core liners. Three core liners split (3H, 5H, 7H), and two of them had to be pumped out of the core barrel. While pulling the core barrel out of the sediment during Cores 5H, 6H, and 7H, the overpull was 20,000 to 35,000 lb.

XCB Cores 8X through 19X were taken from 3454.5 to 3570.1 mbrf (62.3–177.9 mbsf), coring 115.6 m and recovering 60.63 m (52.4%). The overall APC/XCB recovery was 69.0%.

In preparation for logging, we circulated 20 barrels and then 30 barrels of sepiolite mud, and pulled the pipe up to 63 mbsf with negligible overpull. While lowering the pipe to the bottom of the hole, there was 30,000-lb drag to 85 mbsf. We therefore decided to place the bottom of the pipe at about 90 mbsf for logging. We encountered 15 m of hard fill in the bottom of the hole, dropped the go-devil to open the LFV, and circulated 30 barrels of sepiolite mud to clean the fill out of the hole. The pipe was then pulled back up to 3482.0 mbrf (89.8 mbsf) for logging below the unstable section. The Quad-combo tool was run in the hole but could not pass 3492.0 mbrf (99.8 mbsf), or about 10.0 m below the bit, so we retrieved the logging tool. We then reamed out the hole from 3482.0 to 3521.3 mbrf (89.8–129.1 mbsf) through the unstable debris-flow section, using up to 15,000-lb wob, but the hole had collapsed and required drilling to clean out; the logging attempt was canceled. The bit cleared the seafloor at 2350 hr 7 May.

Hole 941B

We moved the ship 300 m south of the beacon or about 490 m in a direction 154° from Hole 941A, positioned the bit at 3386.0 mbrf, and Hole 941B was spudded at 0133 hr 8 May. Core 1H recovered 6.60 m, and the mud line was defined to be at 3388.9 mbrf. Cores 1H through 12H were taken from 3388.9 to 3474.0 m (0–85.1 mbsf) and recovered 96.09 m (112.9%; Table 1). While taking Cores 6H through 12H, we used the advance-by-recovery method. Parts of Cores 2H, 3H, 4H, 5H, 6H, 8H, 10H, 11H, and 12H were disturbed as a result of either gas-induced extrusion of core from the liner onto the rig floor or collapsed core liners. Seven of the core liners had to be pumped out of the core barrel. Cores 3H through 12H were oriented using the Tensor tool.

The primary objective of coring at Site 941 was to obtain undisturbed samples from the surficial debris flow. XCB cores from debris flows at other Leg 155 sites had been disrupted by the XCB coring process. The unusually stiff, dry clay in the debris flow had forced the change to XCB coring sooner than expected in Hole 941A, and XCB recovery was poor initially. We then decided to force the APC system deeper in Hole 941B. We coated the interior and exterior of the butyrate core liners (starting with Core 3H) with a mixture of 1 quart of Minex drilling lubricant (polymer) and 5 gal fresh water. We did this to try to facilitate entry of the core into the liner and to help with removal of the liner from the core barrel when the stiff clay expanded. The lubricant could be felt on the liner after the core was retrieved, indicating that some of the polymer remained on the core liner after the wireline trip to bottom. However, seven of 12 cores had to be pumped out, and this test was not considered successful. The bit cleared the seafloor at 1615 hr and cleared the rig floor at 2155 hr 8 May.

LITHOSTRATIGRAPHY

Introduction

At Site 941, 177.92 m was cored in two holes (Fig. 5). Recovery was especially poor from ~65 to ~130 mbsf (Cores 941A-8X through -14X). Part of this recovery problem was caused by the splitting of plastic liners during coring. Hole 941B recovered some of this missing section (~65–85 mbsf, Cores 941B-8H through -12H) by taking only 5-m-long cores with the APC; this procedure seemed to alleviate the problem of split core liners. However, Hole 941B is offset about 500 m from Hole 941A.

Gas expansion and escape disrupted sedimentary structures of some of the thicker silt and sand beds particularly within the lowermost unit. In addition, drilling disturbance formed "biscuits" in some of the XCB cores, causing deformation and rotation of beds producing "chevron-" and "wood-grain"-like fold patterns in the cores (see "Lithostratigraphy" section of "Explanatory Notes" chapter, this volume). This deformation tends to be accentuated in zones of disturbed bedding produced by syn- and post-depositional processes (e.g., slumps, debris flows, etc.); however, it can complicate distinguishing in-situ structures from drilling disturbance. The sedimentary section is divided into four major lithologic units: Units I to IV (Fig. 5).

Description of Lithostratigraphic Units

Unit I

Intervals: 155-941A-1H-1, 0–98 cm; 155-941B-1H-1, 0–66 cm
Age: Holocene
Depth: 0.00 to 0.98 mbsf (Hole 941A); 0.00 to 0.66 mbsf (Hole 941B)

Unit I consists of brown calcareous clay (10YR 5/3) with abundant foraminifers and nannofossils that grades downward into light brownish gray (2.5Y 6/2) foraminifer-bearing clay. The sediment is moderately bioturbated and slightly color mottled. The carbonate content is 31.9% at 0.18 mbsf in the upper part of the unit, but sharply decreases downward to 1.9% at 1.75 mbsf in the upper part of Unit II. Interval 941A-1H, 46–63 cm, consists of foraminifer sand with abundant pteropods and other shell fragments (Fig. 6). This deposit is not present in Hole 941B and may partially account for Unit I being 32 cm thicker in Hole 941A than in Hole 941B. This foraminifer sand appears to be the deposit of a turbidity current or related gravity-con-

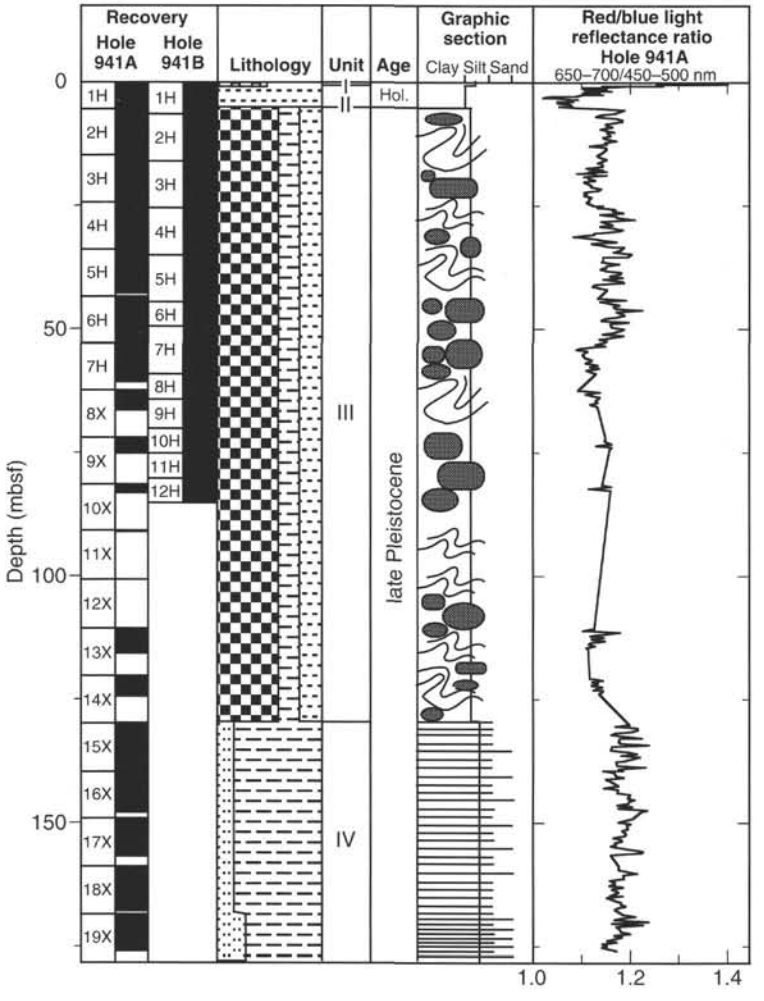

Figure 5. Composite stratigraphic section for Site 941 showing core recovery, a simplified summary of lithology, depth of unit boundaries, age, a graphic section with generalized grain-size and bedding characteristics, and downhole variations in light-reflectance values. The lithologic symbols are explained in Figure 1 of the "Explanatory Notes" chapter, this volume. The stippled objects in Unit III (graphic lithology section) represent large sedimentary clasts.

trolled process because (1) well-sorted, sand-size foraminifers are present, whereas clay- and silt-size particles (including juvenile foraminifers) are absent or rare; (2) pteropods are abundant, even though this deposit is well below the aragonite compensation depth (~1400 m); (3) the bed has a sharp base; (4) the bed does not occur in Hole 941B only 500 m away; and (5) the carbonate content of the bed is anomalously high (79.2%) compared to the carbonate content of the rest of the unit, indicating an absence of terrigenous sediment in this bed. Although the lithology of Unit I is the same as in the uppermost units at the other Leg 155 sites, neither hole at this site contains the distinctive iron-rich, rust-colored, diagenetic crust that is developed in Unit I at most of the other drill sites (e.g., Fig. 6 of "Site 930" chapter, this volume).

Unit II

Intervals: 155-941A-1H-1, 98 cm, through -1H-CC, 21 cm; 155-941B-1H-1, 66 cm, through -1H-CC, 19 cm
Age: Holocene to (?)late Pleistocene
Depth: 0.98 to 5.30 mbsf (Hole 941A); 0.66 to 6.60 mbsf (Hole 941B)

Unit II consists of terrigenous, gray to dark gray clay to silty clay of slightly different colors in each hole. No silt or sand laminae or beds are present in either hole. Most of the sediment in this unit is stained to varying degrees by diagenetic hydrotroilite, which generally imparts an ephemeral black color (N 2/0) to the sediment as irregular, faint patches, but in some sections completely stains the sediment black (N 1) (see "Introduction" chapter, this volume). The carbonate content is low (0.6% to 5.7%) throughout the unit.

Unit II in Hole 941A contains smooth gray clay (5Y 5/1) at the top that abruptly changes to very dark-greenish gray clay (5GY 3/1) at 2.43 mbsf and continues to the base of the unit. The entire interval is only faintly color-mottled by hydrotroilite staining, except for 1.90 to 2.05 mbsf, where the entire core is intensely stained. The most unusual features encountered in Unit II of Hole 941A are large, very pale brown (10YR 7/3) to yellowish brown (10YR 5/6) crystals at 941A-1H-3, 88–92 cm, and -3, 7–15 cm (Fig. 7). These crystals are interpreted as diagenetic ikaite ($CaCO_3 \cdot 6H_2O$; see "Inorganic Geochemistry" section, this chapter).

In Hole 941B, Unit II consists of olive gray clay (5Y 5/2 to 5Y 4/2) at the top, becoming greenish gray (5GY 5/1) below. Parts of the interval are moderately bioturbated, and the clay becomes silty in the lower part of the interval. The clay is faintly color-mottled by hydrotroilite, except for the interval 941B-1H-4, 9 cm, through -1H-5, 43 cm, which is completely black (N 2/0). Upon exposure to air, this black stain on the split core surface disappeared (oxidized) in about 8 hr.

Unit III

Intervals: 155-941A-2H-1, 0 cm, through -15X-1, 0 cm; 155-941B-2H-1, 0 cm, through -12H-CC, 81 cm (bottom of the hole)
Age: late Pleistocene
Depth: 5.30 to 129.70 mbsf (Hole 941A); 6.60 to 85.10 mbsf (Hole 941B)

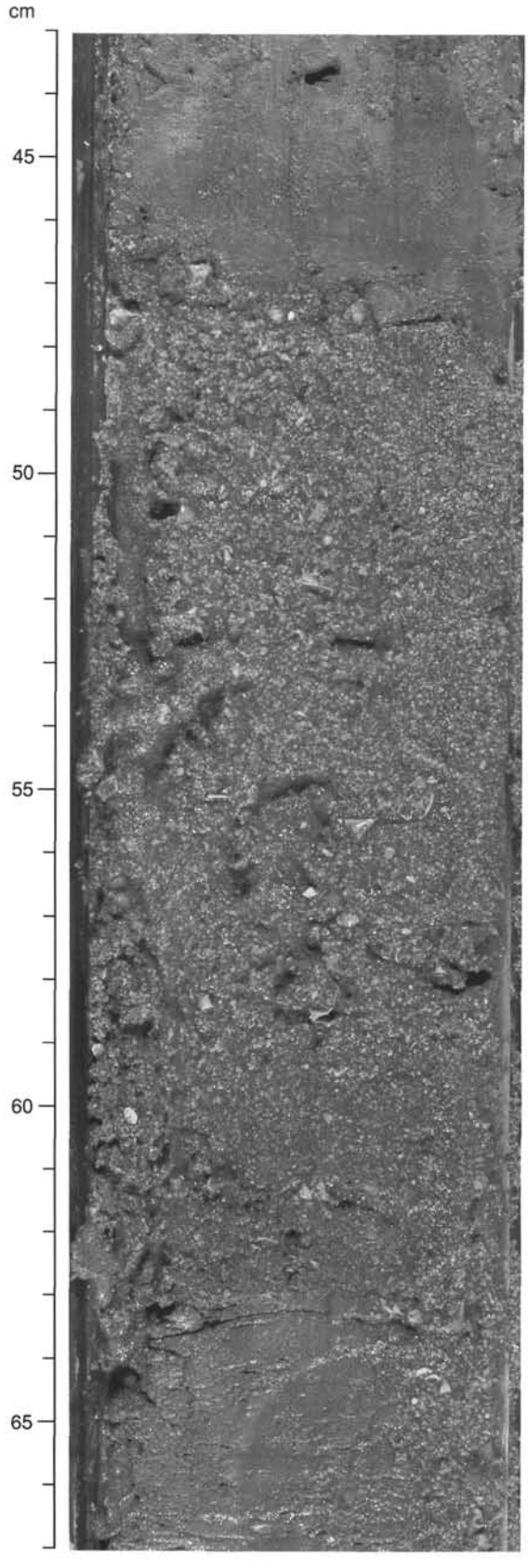

Figure 6. Redeposited bed of foraminifer sand with abundant pteropods (47–63 cm) in Unit I (155-941A-1H-1, 43–67 cm).

Unit III is a thick sequence of clay and silty clay of variegated color ranging through shades of dark gray (5Y 4/1, 5Y 3/1, 10Y 3/1), dark olive gray (5Y 3/2), dark greenish gray (5GY 3/1, 5GY 4/1, 5GY 5/1), and black (5GY 2.5/1, 5Y 2.5/1, N 2/0; Figs. 8 through 22). Textures of the clay components range from very soft, smooth, and homogeneous to very dense and stiff. Some have a shiny, greasy, or glossy appearance, whereas other clay units have a rough surface caused by dispersed sand grains. The carbonate content is generally low (2%–3%) throughout the unit, but is higher (up to 6.8%) in a few isolated samples (see "Organic Geochemistry" section, this chapter). In contrast to the units above and below, core recovery within Unit III was poor (53%; Fig. 5).

Virtually all cores from Unit III have been affected by soft-sediment failure, deformation, and redeposition as evidenced by abrupt changes in lithology and color, structures indicative of deformation such as folds and faults, discordant stratal relationships between dipping laminae, beds and lithologic contacts, and the occurrence of clasts of various sizes. No clear lithologic subdivisions could be recognized in the unit, and no distinctive lithologies, discrete beds, or structures could be correlated between holes. The following is a brief description of some of the representative lithologies and features observed in this thick, deformed unit. For more comprehensive descriptions of individual cores or sediment intervals within the unit, consult the visual core descriptions (VCD) in the "Cores" chapter, this volume, and the section-by-section handwritten sedimentological core description sheets available from ODP.

Dipping color bands, laminae, beds, and contacts are ubiquitous in Unit III (Figs. 8 through 15). Dips range from very slight to nearly 90°, and dips of 50° to 80° are common. In some cores, as well as in a few individual core sections, groups of laminae and/or beds clearly dip at different attitudes and directions indicating the occurrence of discordant stratal relationships (Figs. 9 and 13A). In most cases, the actual contact between discordant beds is subtle. In a few cases, however, clearly defined contacts appear to be faults (Figs. 12, 13, 14). These relationships indicate that Unit III is composed of discrete, detached, commonly deformed blocks or clasts of variable size ranging from centimeters to at least several meters in scale.

Also observed are various scales of folds, which further indicate that soft-sediment deformation has occurred throughout the unit. Only a few small folds on the scale of centimeters are visible in the cores (Figs. 9, 15, 16, 22); these are rarely isoclinal and recumbent (e.g., Fig. 22). Some of these small folds may be the cores of larger folds. Intervals 941A-2H-5, 120 cm, through -6, 50 cm; 941A-5H-4, 25–100 cm (Fig. 15); and 941B-9H-3, 10–100 cm, provide good examples of folds at a decimeter scale that either are clearly visible in the core or can be reasonably inferred to exist based on the attitudes of the beds in these intervals. Further evidence to suggest folding of the sediment, as well as faulting or shearing, is the deformed nature of most of the color bands, laminae, and beds of this unit. Most of these bands and beds appear squeezed or stretched and have irregular boundaries that appear as "crenulated" patterns (Figs. 8 through 10, 12, 13, 17), and many lithologic boundaries appear to show small-scale faults with displacements on the order of centimeters or less (Figs. 12, 13, 14, 17, 18A), which suggest brittle deformation associated with larger scale folding.

Rare larger folds up to several meters in scale can be inferred from the attitudes of dipping beds in the cores. In interval 941A-3H-4, 0–130 cm, beds and laminae dip in one direction at the top and the opposing direction at the bottom. Paleomagnetic analysis indicated a change in polarity between these segments with opposing dips. Thus, this interval appears to contain a large fold. These types of observations suggest that many of the intervals of steeply dipping beds observed within the cores may be sediment within the limbs of large folds.

A variety of clasts occurs throughout Unit III. Shell fragments including echinoderms (Figs. 14 and 20), gastropods, pteropods (Fig.

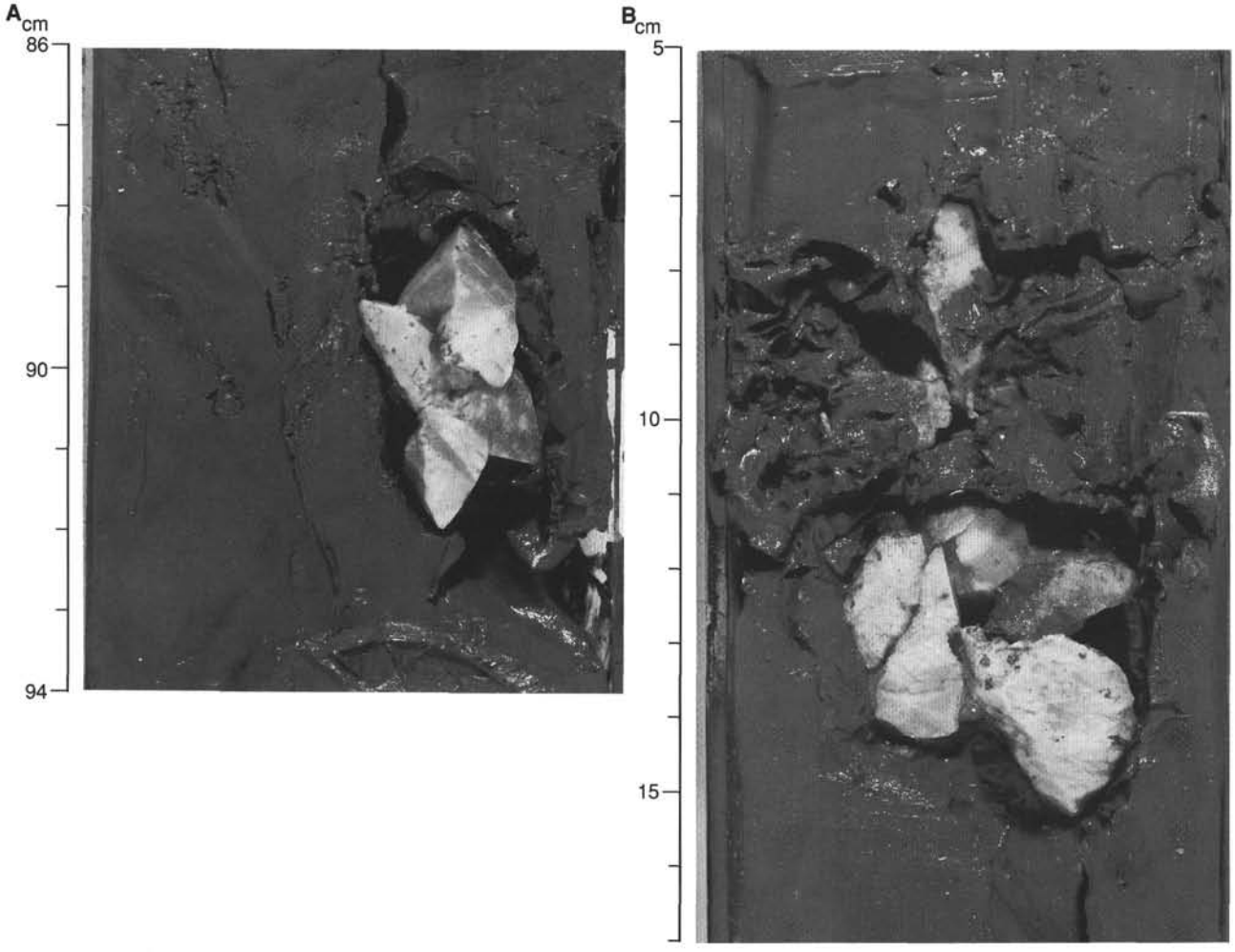

Figure 7. Crystals of ikaite ($CaCO_3 \cdot 6H_2O$) in Unit II. **A.** Interval 155-941A-1H-3, 86–94 cm. **B.** Interval 155-941A-1H-3, 5–17 cm.

12), ostracodes, and other unidentified aragonitic fragments (Figs. 11, 14, and 15) occur throughout the unit, but only the echinoderm fragments are so common that they are present in most cores. Wood fragments are rare; however, fine organic detritus is disseminated in some zones, and a large piece of wood, 3.5 × 3 × 1 cm in size, was found at interval 941B-8H-CC, 3–7 cm.

Clasts of lithified sediment such as siltstone (Fig. 21) and rock pebbles (Fig. 20) occur rarely. Small clasts of unlithified silt and sand occur in a few intervals (Fig. 22). Such silt/sand clasts are commonly deformed and oriented parallel to the dipping beds of the surrounding clasts (Fig. 22; see also intervals 941B-9H-03, 80–95 cm, and -7H-5, 5 cm, through -7H-6, 20 cm). These oriented clasts are clearly silt and fine sand laminae and beds, which have been disrupted and deformed and indicate that overbank deposits of channel-levee systems of the fan have been incorporated into the sediment of Unit III. Silty and sandy intervals, however, are extremely rare throughout the unit.

Discrete mud clasts of various sizes, colors, and shapes are abundant in some sections. Most of the sediment composed of mud clasts is clast supported with little apparent matrix (Figs. 17, 18, 19). Isolated clasts within a clay matrix are less common, and some are hard to distinguish from the matrix (Figs. 9, 10, 12, 13). Clasts are commonly deformed with "crenulated" and serrated boundaries that indicate they are microfaulted or sheared (e.g., Figs. 17 and 18). Clasts commonly show a variety of colors, textures, and compositions (Figs. 17, 18, 19). For example, two clasts (Figs. 18A and 19) have carbonate contents substantially higher than average values. Mud clasts apparently range in size from centimeter-scale clasts, which are clearly recognizable in the cores, up to meter-scale or larger clasts (i.e., blocks) that span more than one core section.

The base of Unit III apparently was not recovered and is between Sections 941A-14X-CC and -15X-1, 0 cm.

Unit IV

Intervals: 155-941A-15X through -19X (bottom of the hole)
Age: late Pleistocene
Depth: 129.70 to 177.90 mbsf

Unit IV consists of very dark gray (5Y 3/1, 5Y 4/1) to dark olive gray (5Y 3/2) silty clay with numerous discrete laminae and beds of silt (Figs. 5, 23, 24); sand-size particles do not appear to be present in any of these laminae or beds. Most of the clay intervals between silt laminae and beds show faint, black, hydrotroilite-rich, horizontal color bands or laminae. A few short intervals where silt laminae and beds are less common show faint color mottling and appear to be slightly bioturbated.

Approximately nine to 10 silt laminae thicker than 1 mm occur per meter of core in Cores 941A-15X through -17X, six per meter in -18X, and 22 per meter in -19X. Some intervals of sediment also have numerous, very thin (<1 mm), commonly discontinuous silt laminae (Figs. 23 and 24), which are not included in the counts of layers per meter. Beds of silt average 1–2 cm in thickness, but range up to 7 cm.

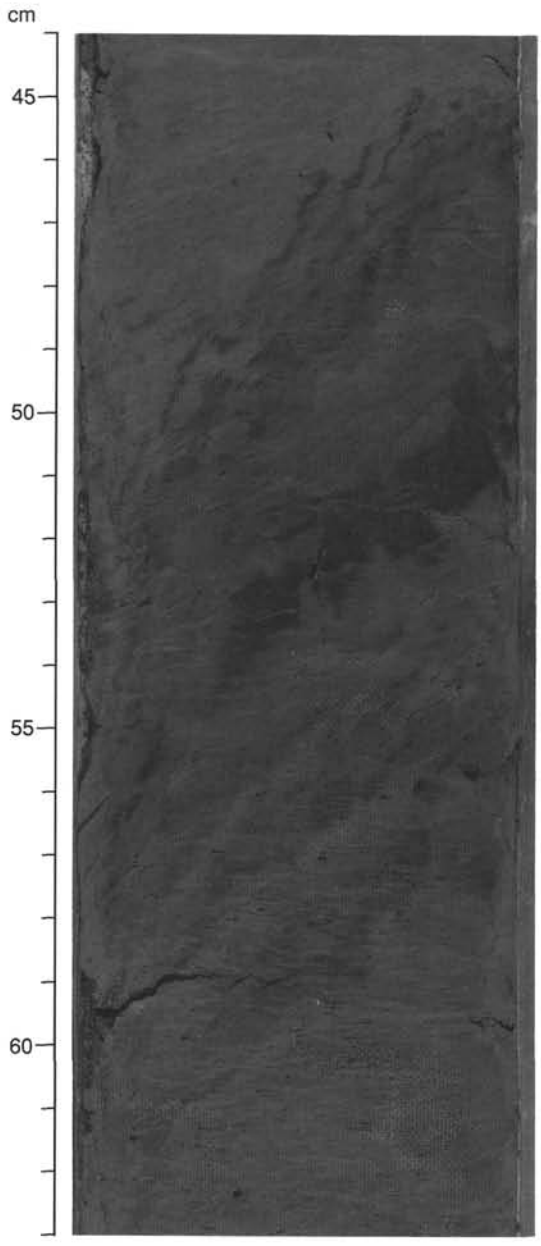

Figure 8. Steeply dipping, "crenulated," deformed color bands and beds in Unit III (155-941A-3H-6, 44–63 cm). Subhorizontal streaks are artifacts from scraping the core surface.

Beds are much less common than laminae and average two to three beds per meter in Cores 941A-15X through -17X and less than one per meter in Core -18X. Beds increase to eight per meter in Core 941A-19X at the bottom of the hole.

Many of the silt laminae and beds exhibit parallel- or cross-lamination (Figs. 23 and 24). Many of the silt beds, as well as some of the laminae, appear normally graded with sharp, irregular bases and gradational tops (Fig. 24). Some grade upward from silt into alternating laminae (~1 mm thick) of silt and mud, and finally into mud.

Mineralogy

Mineralogy was determined by estimation of mineral volume percentages in smear slides and by X-ray-diffraction (XRD) analysis of samples of silty clay.

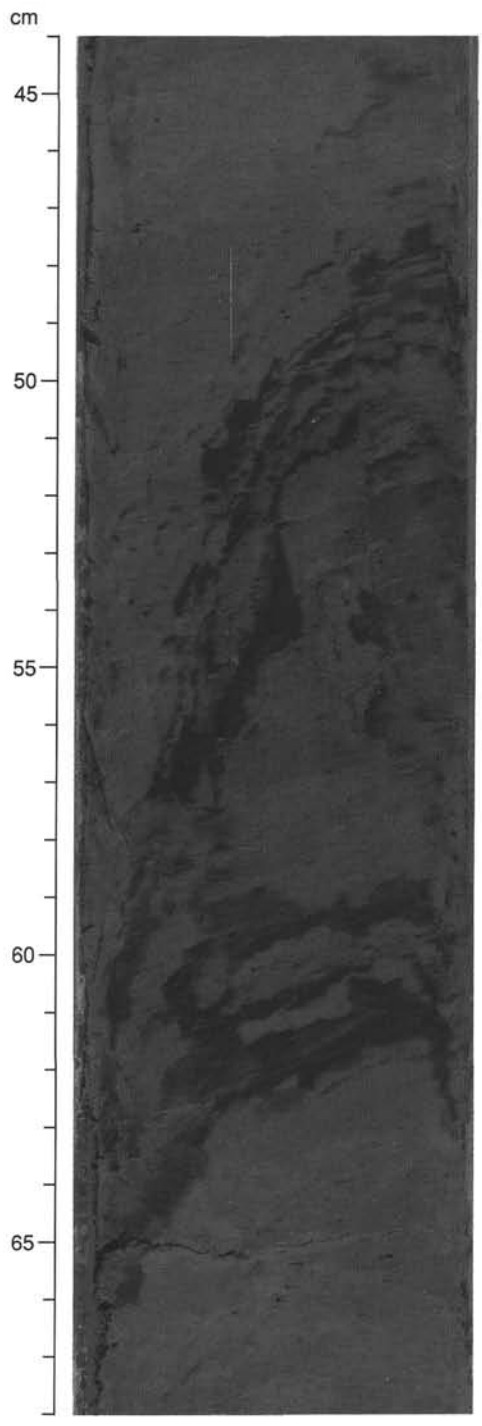

Figure 9. Steeply dipping, "crenulated," deformed color bands and beds in Unit III. A discordant lithologic contact may occur at about 58–60 cm. The dark- and light-colored interval from 59 to 63 cm may be a fold or deformed clasts (155-941A-3H-7, 44–68 cm).

Smear-slide Synthesis

Silty clay of Unit II consists of 75%–82% clay and 18%–25% silt. The silt fraction is about 60% quartz, 6%–8% feldspar (mainly plagioclase), 6%–8% mica, and 20%–30% accessory minerals. Organic detritus, foraminifers, and sponge spicules compose less than 3% of the sediment, and nannofossils about 1%.

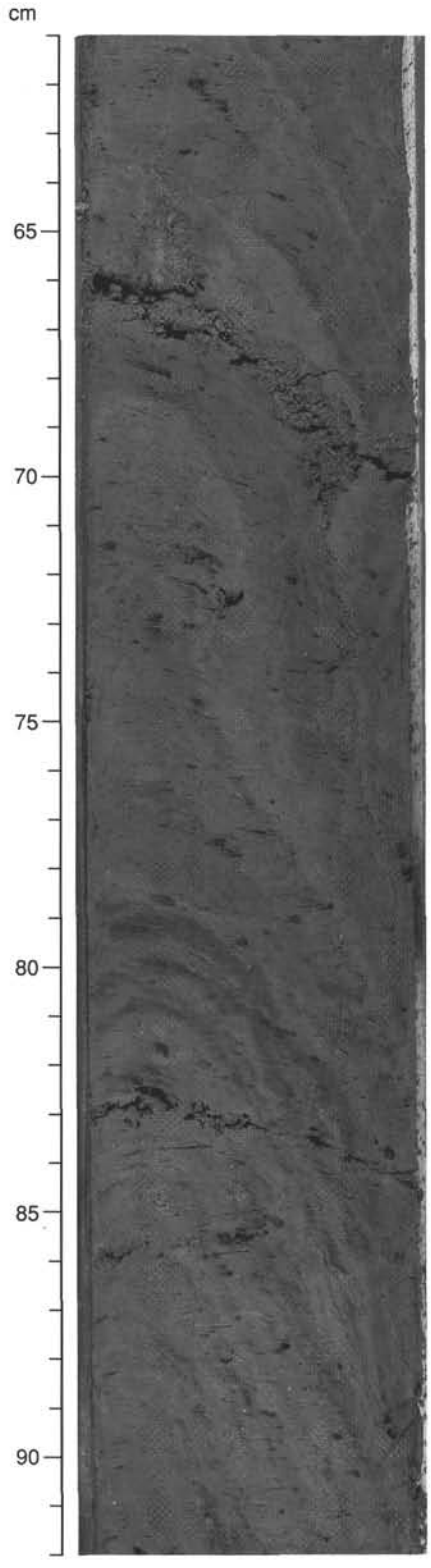

Figure 10. Steeply dipping, "crenulated," faulted color bands and beds in Unit III. Some beds may be deformed mud clasts. A lamina of foraminifer sand dips from left at 63.5 cm to right at 78 cm (155-941A-4H-3, 61–92 cm).

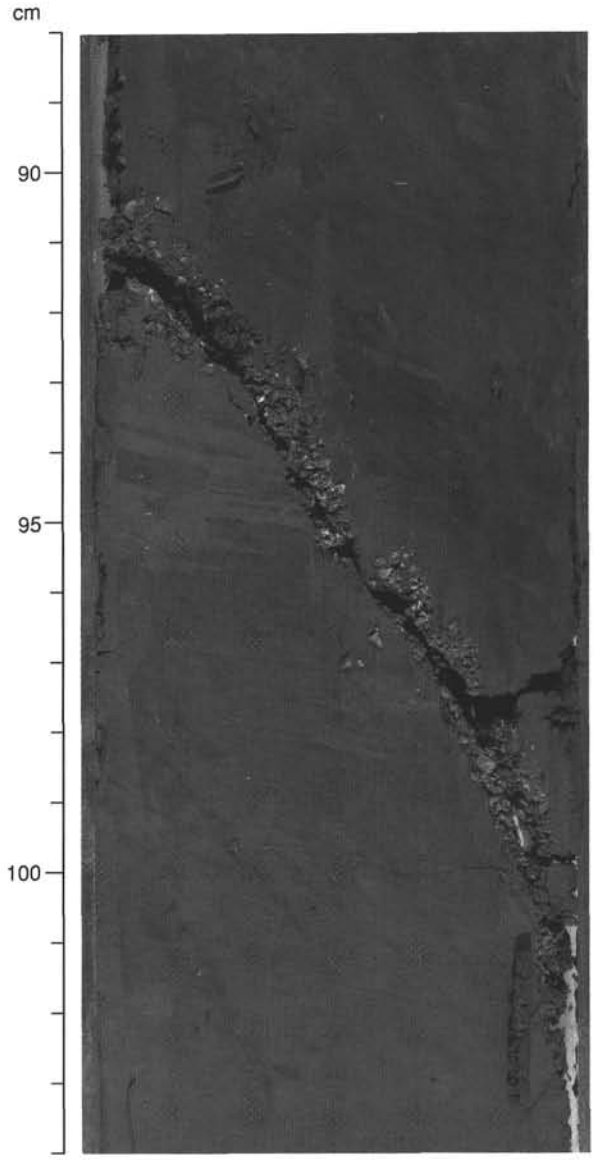

Figure 11. Steeply dipping lamina of shell fragments in a block or clast of black silty clay in Unit III (155-941B-11H-3, 88–104 cm).

Fine to coarse sand clasts in Unit III consist of about 70% quartz (mainly monocrystalline), 3%–15% feldspar (mainly plagioclase), 1%–7% mica, 1%–5% combined amphibole and pyroxene, and 1%–5% opaque minerals. The opaque grains include hydrotroilite and unidentified oxides. About half of the quartz and feldspar grains are well rounded with surface coatings of iron oxide. This distinguishes them from the fine sand grains in the clasts, which are angular to subangular.

Unit IV is predominantly silty clay (28%–47% silt, 53%–72% clay) and rare foraminifers, nannofossils, sponge spicules, and organic detritus.

XRD Data

Based on the relative intensities of primary diffraction peaks, the main mineralogical components of 16 silty clay samples are quartz, plagioclase, augite, and the clay minerals smectite, illite (+ mica), and kaolinite (Table 2; Fig. 25). A few samples contain K-feldspar.

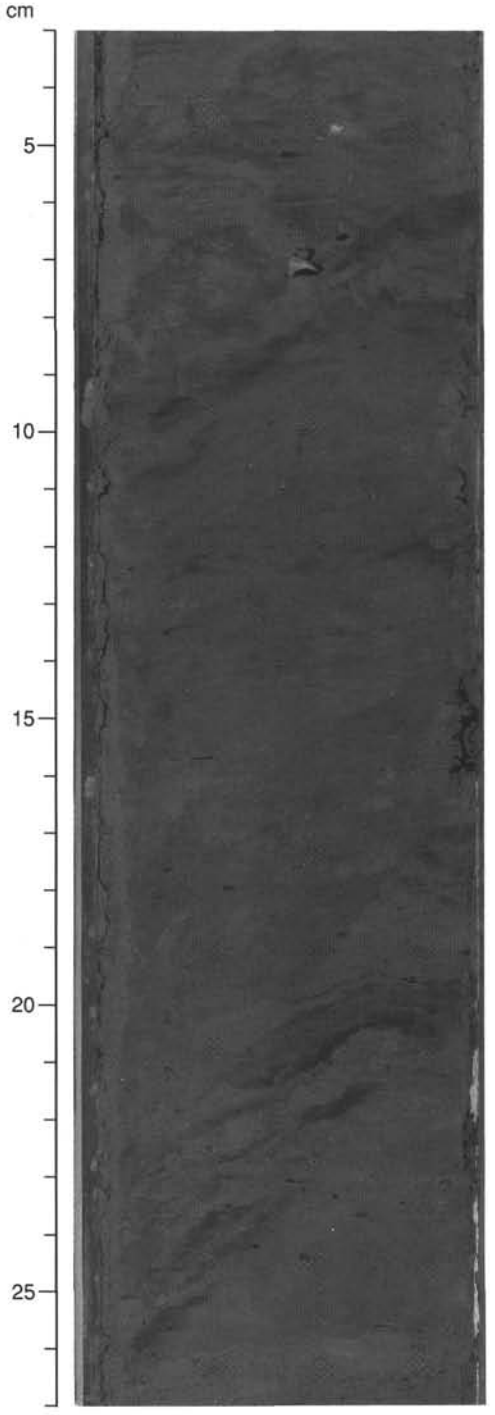

Figure 12. Dipping fault (from right at 16.5 cm to left at 23.5 cm) bounding large clasts in Unit III. Pteropod shell fragments occur between 4 cm and 7 cm. Faint deformed clasts occur from 5 to 10 cm (155-941B-4H-2, 3–27 cm).

Because of the heterogeneous character of the Unit III mass-transport deposits, mineral composition fluctuates erratically from about 20 to 130 mbsf. In Unit IV (130 to 178 mbsf), the content of clay minerals (+ micas) increases steadily with depth. Feldspar content also appears to increase near the base of the cored succession.

The relative proportions of clays are quite variable at Site 941, particularly in the mass-transport deposits of Unit III (Fig. 25B).

Spectrophotometry

Reflectance of visible light was low throughout the sediment column recovered at Site 941. For all wavelength bands from 400 to 700 nm, reflectance values range from 10% to 28% in Units II through IV, and reach 35% in the red spectrum at the top of Unit I. The ratio between red (650–700 nm) and blue (450–500 nm) spectral reflectance averages 1.15 (Fig. 5). The most prominent contrast in the red/blue ratio is associated with the occurrence of either iron sulfides or iron oxyhydroxides. The interval of very dark greenish gray (5GY 3/1) clay from 2.43 to 5.30 mbsf in Unit II contains iron sulfide and is characterized by the lowest red/blue ratio recorded at Site 941. The highest red/blue ratio of 1.6 corresponds to the brown (10YR 5/3) calcareous clay of Unit I, where red reflectance is enhanced by iron oxyhydroxides.

Units III and IV differ slightly in their mean red/blue ratio. The variability in the red/blue ratio within lithologic Unit III is apparently related to the ephemeral and irregular variation and intensity of color banding or mottling, as well as to the occurrence of mud clasts of variegated color, and gas partings. In Unit IV, the increased content of silt layers enhances red (650–700 nm) reflectance, but monosulfide staining must also account for some changes in the red/blue ratio, because the coarse sampling interval (40 cm) resulted in many of the thin silt layers being excluded from the reflectance measurements.

Discussion

Site 941 was drilled into a regionally extensive mass-transport deposit that occurs at or very near the present-day seafloor on the western part of the Amazon Fan. This unit has been interpreted previously as a debris-flow deposit based on seismic, GLORIA side-scan sonar, and piston-core data (Damuth and Embley, 1981; Damuth et al., 1988; see "Setting and Objectives" section, this chapter). Hole 941A penetrated the entire thickness of this deposit. Unit IV is a sequence of silty clay with numerous graded silt laminae and beds from beneath the debris-flow deposit. This sequence apparently represents overbank turbidites within the (?)Purple Channel-levee System of the Upper Levee Complex.

Unit III, which corresponds to the acoustic unit interpreted as debris flow on seismic profiles, consists of a clast-supported sedimentary breccia composed of silty clays of variable lithologies that have been folded, faulted, and otherwise deformed by soft-sediment deformation. The occurrence of clasts and blocks of various sizes suggests deposition by a debris flow(s), whereas the occurrence of folds of various scales suggests deposition by muddy slumps. Whether one or both of these processes occurred and whether more than one depositional event is responsible for this deposit are uncertain. Many clasts within the deposit indicate that the sediment was derived mainly from shelf or slope areas (e.g., clasts containing pteropods, ostracodes, and other aragonitic shell fragments). Some clasts, however, indicate that slumped Amazon Fan deposits may compose a small amount of the sediment.

Unit II consists of a thin deposit of gray hemipelagic silty clay that overlies the mass-transport deposit and that grades upward into the brown, calcareous hemipelagic sediment of Unit I, which apparently records the rather abrupt decrease in terrigenous sediment supply to the entire Amazon Fan in response to sea-level rise at the beginning of the Holocene (e.g., Damuth, 1977).

BIOSTRATIGRAPHY

Calcareous Nannofossils

Abundant and well-preserved nannofossils are present in the nannofossil-foraminifer clay of Unit I. The microfossil assemblage includes relatively abundant juvenile foraminifer tests (20–30 µm)

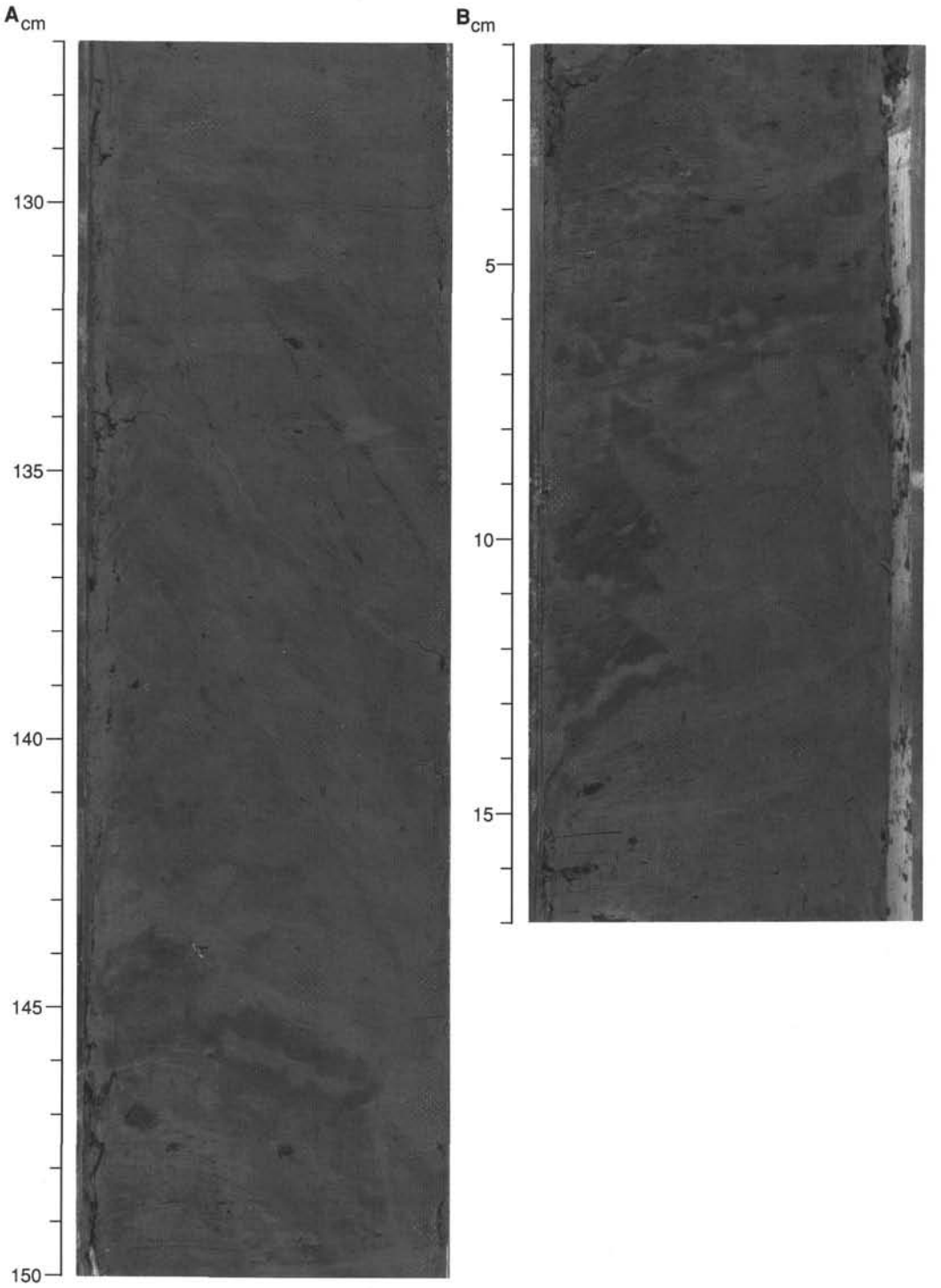

Figure 13. **A.** Steeply dipping color bands and beds in Unit III overlie a deformed, faulted lithologic boundary of a mud clast, from left at 144 cm to right at 148 cm (155-941A-6H-2, 127–150 cm). **B.** Basal portion of the black mud clast in (A) showing a very serrated boundary (from right at 7 cm to left at 14 cm) caused by microfaulting (155-941A-6H-3, 1–17 cm).

filled with black authigenic minerals. High abundances of well-preserved nannofossils are found in Unit II to a greater depth (1.4 mbsf, Sample 941A-1H-1, 143–148 cm) than seen at previous sites. Below 1.4 mbsf of Unit II and in Units III and IV nannofossils have a low abundance (Samples 941A-1H-CC, 20–21 cm, through -19X-CC, 27–28 cm). The sporadic occurrence of *E. huxleyi* places the glacial-age sediment of these units in nannofossil Zone CN15. Nannofossils were found in higher concentrations in some of the reworked clasts within Unit III. The clasts sampled in the upper part of the debris flow (Unit III) were barren of nannofossils (e.g., Samples 941A-3H-5, 27 cm, and -7, 70 cm). In the upper part of Core 941B-4H numerous clasts contained well-preserved nannoflora from nannofossil Zone CN15. Olive green clasts from the lower part of Core 941A-4H and the upper part of Core 941A-5H contained a rich nannoflora dominat-

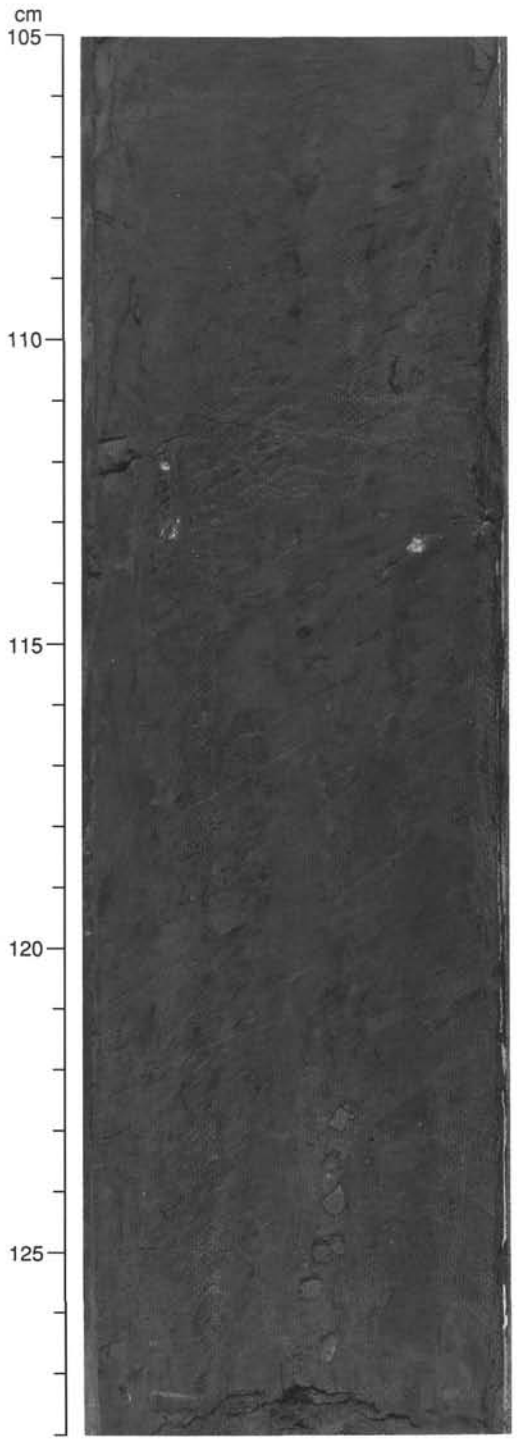

Figure 14. Very steeply dipping fault or lithologic boundary between clasts or blocks in Unit III, extending nearly vertically from right at 105.5 cm to center at 128 cm (155-941B-4H-7, 105–128 cm). Shell fragments between 123 and 128 cm occur along this boundary. White shell fragment on right side at 113.5 cm also occurs along the boundary.

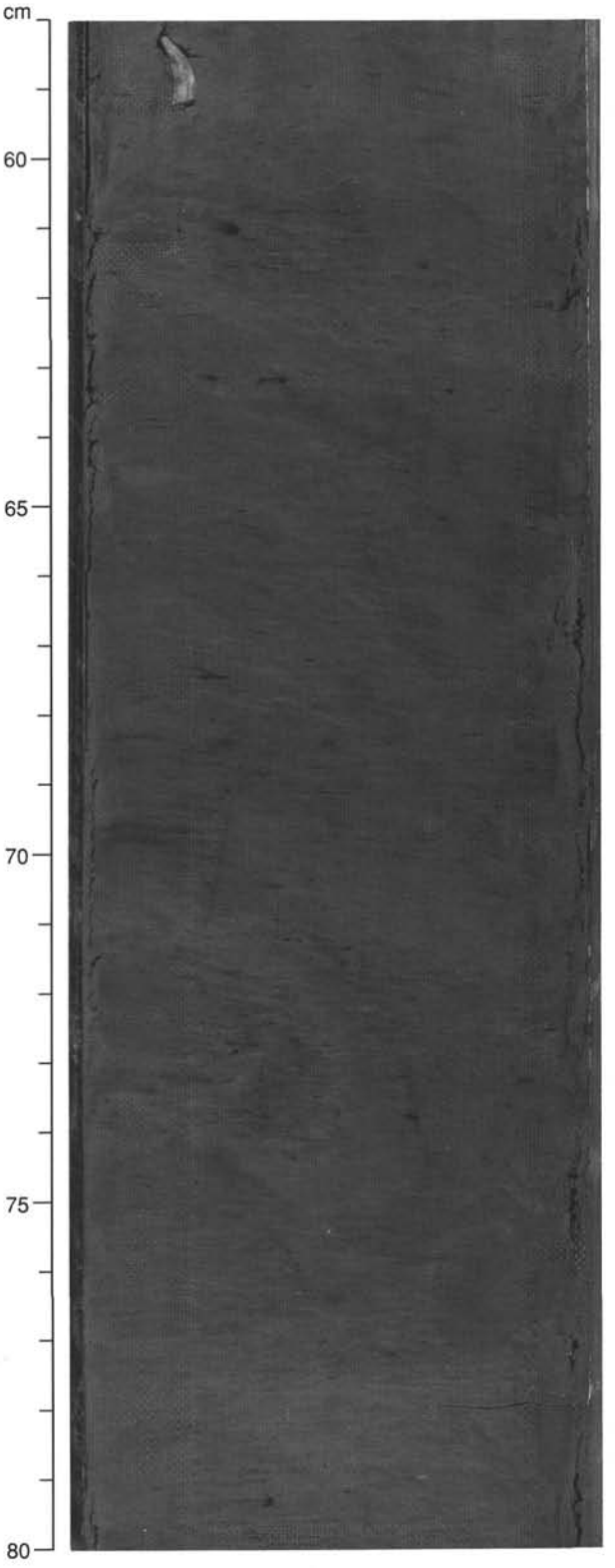

Figure 15. Small isoclinal fold in Unit III (155-941A-5H-4, 58–80 cm). The fold hinge is visible on the left of the core between 70 and 76 cm. The fold extends through the interval 155-941A-5H-4, 20–100 cm (see text). A shell fragment occurs at 58–59 cm.

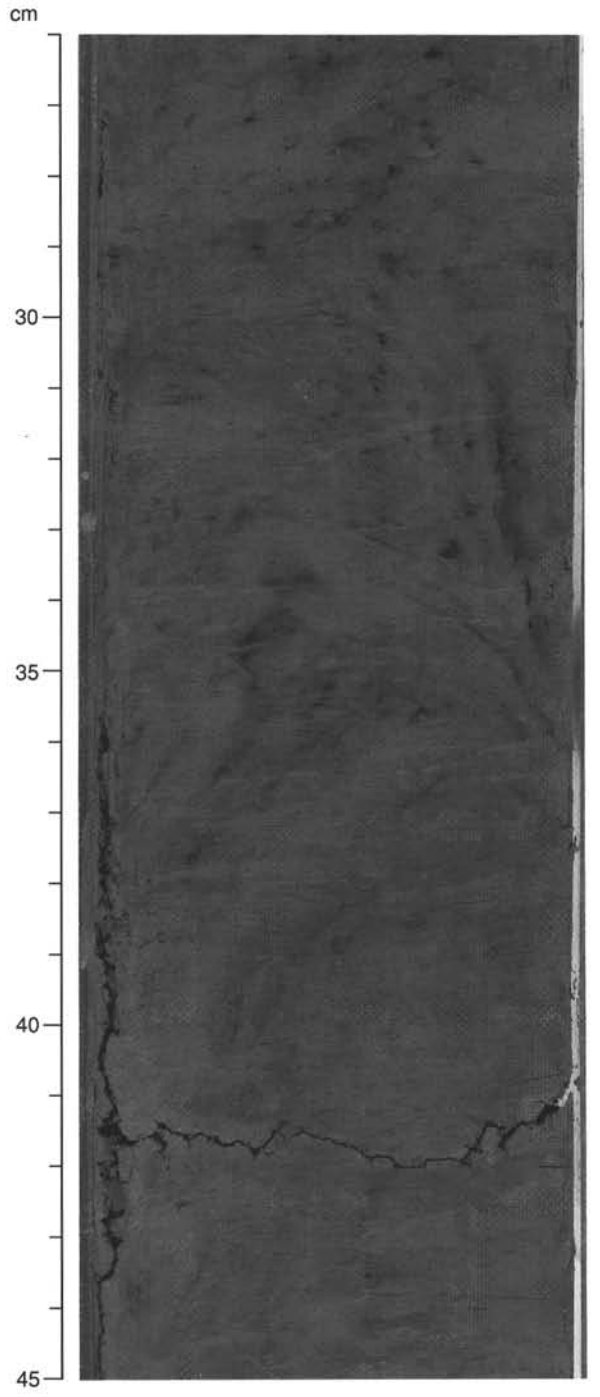

Figure 16. Folded, color-banded layers in Unit III (155-941B-11H-2, 26–45 cm).

ed by species of *Discoaster* of middle and late Miocene ages (Table 3). The majority of reworked clasts in Hole 941B contain Miocene nannofossils.

Planktonic Foraminifers

The boundary between Ericson Zones Z and Y (disappearance of *G. tumida*) cannot be defined at Site 941, as abundant *G. tumida* is found down to the lithostratigraphic boundary between Units II and III (the debris-flow deposit) at 5.3 mbsf (Sample 941A-1H-CC, 21

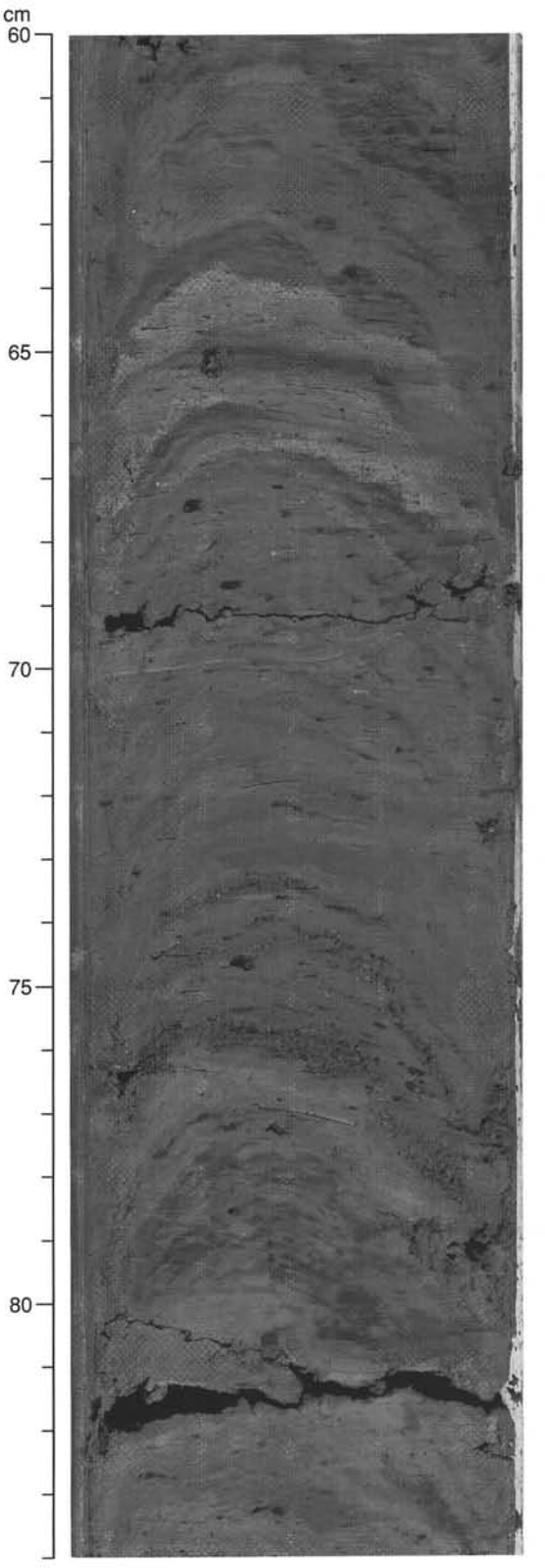

Figure 17. Folded, faulted, and deformed mud clasts of variegated color and contrasting lithologies in Unit III (155-941A-4H-5, 60–84 cm). Lighter colored clasts between 62 and 67 cm have common foraminifers.

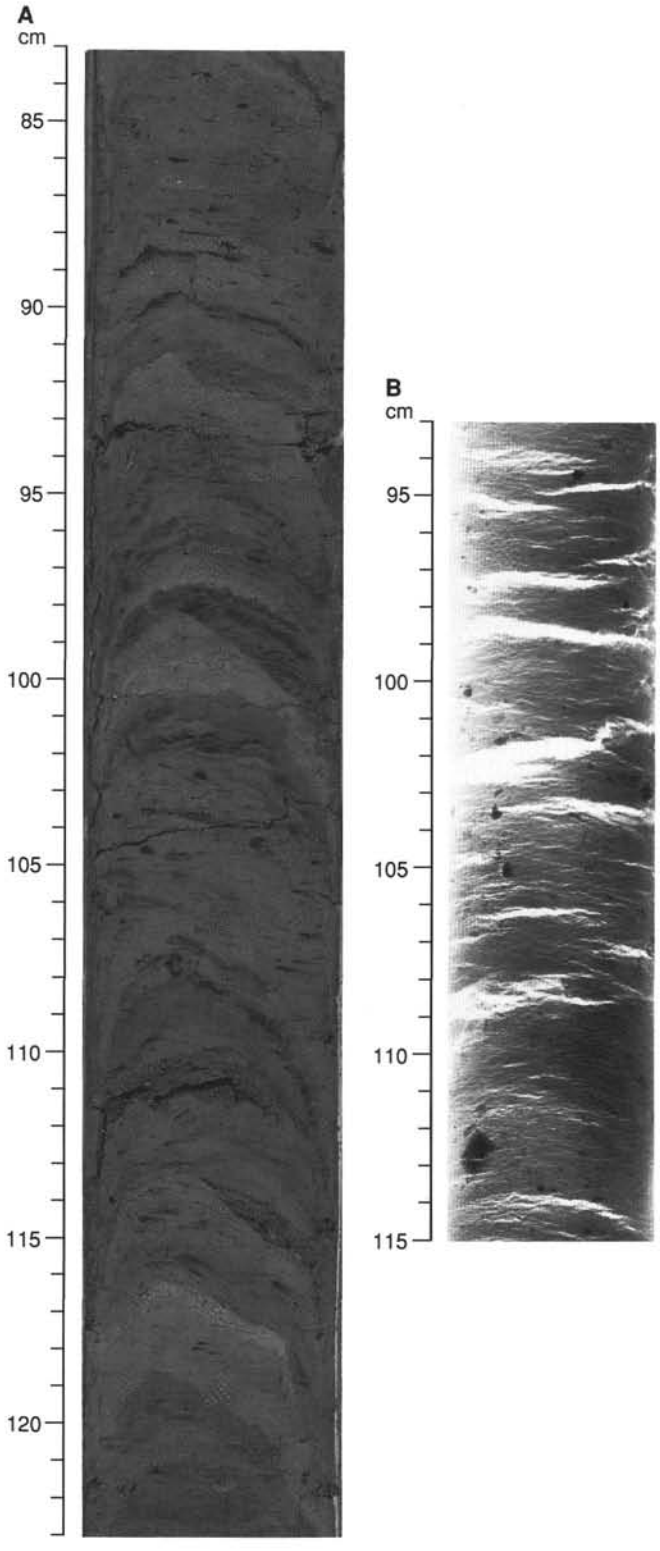

Figure 18. Folded, faulted, and deformed mud clasts of variegated color and contrasting lithologies in Unit III (155-941A-4H-5, 83–123 cm). **A.** The lighter colored clast from 91 to 92 cm has a carbonate content of 6.8%, which is about 2–3 times the average for the unit. **B.** An X-radiograph from 93 to 115 cm shows scattered shell fragments and pebbles. The pebble at 108 cm rests on the split-core surface.

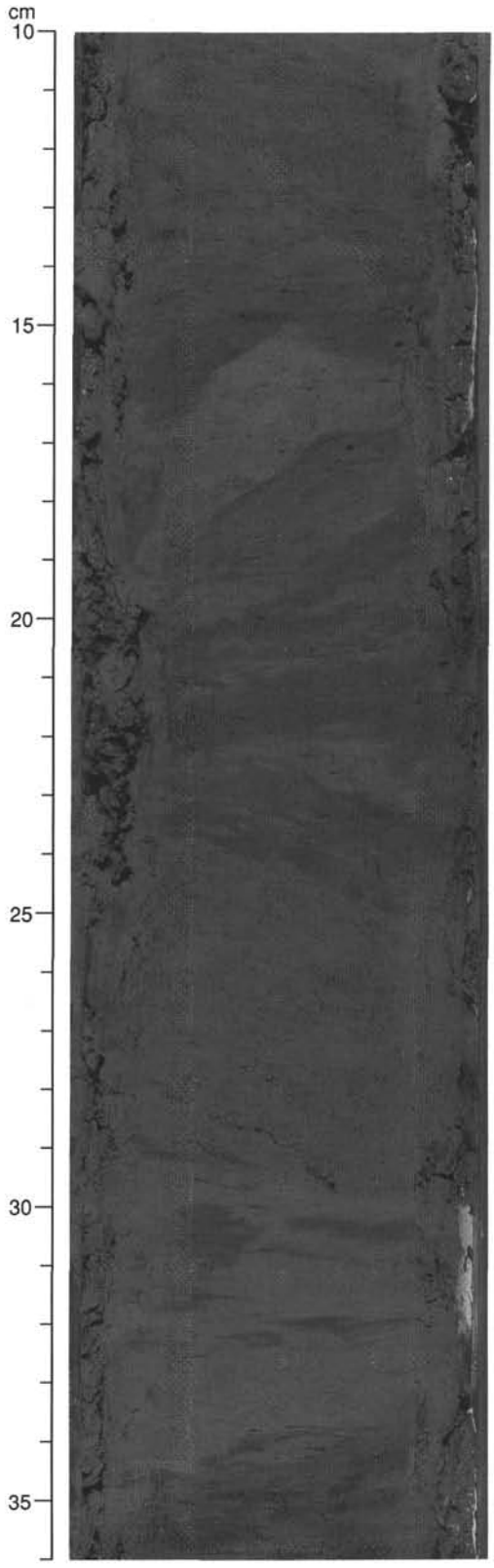

Figure 19. Deformed mud clasts of variable lithology and color in Unit III (155-941A-14X-1, 10–36 cm). Lighter colored clast between 16 and 18 cm has a carbonate content of 5.2%, which is about twice the average for the unit.

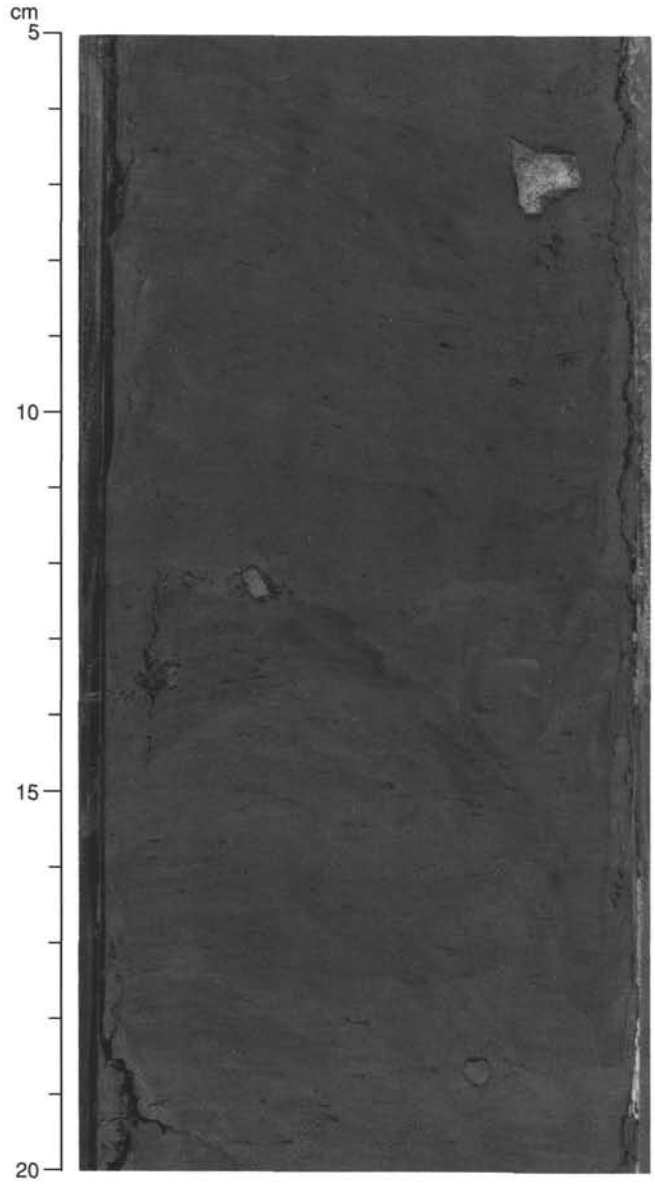

Figure 20. Echinoderm shell fragment (7 cm) and rock pebbles (12 and 19 cm) in Unit III (155-941A-5H-4, 5–20 cm).

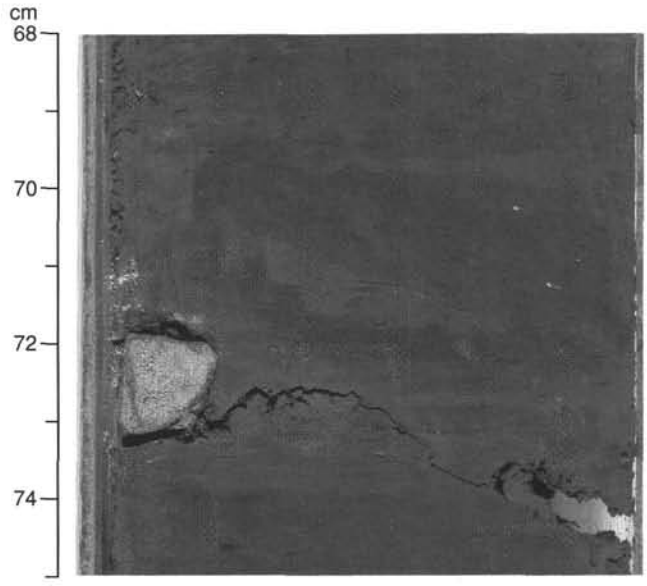

Figure 21. Siltstone pebble in Unit III (155-941B-12H-5, 68–75 cm).

cm). This implies that Holocene (Z Zone) material younger than 9000 yr (the dated reappearance of *G. tumida* in the Atlantic Ocean; G. Jones, pers. comm., 1994) was deposited directly on top of the Unit III debris-flow deposit. Core-catcher contamination could have occurred at Site 941 in the first core, though there are relatively abundant *G. tumida* at 3.63 mbsf (Sample 941A-1H-3, 63–68 cm).

Foraminifer preservation is good in the Holocene interval in Holes 941A and 941B. Sample 941A-1H-1, 50–51 cm (0.5 mbsf), contains high abundances of both planktonic foraminifers and pteropods, all of which are greater than 200 µm, and appears to be a pteropod-foraminifer-rich turbidite. The lower portion of Unit II contains an increasing abundance of authigenic minerals and calcareous spines, suggesting some reworking from the underlying Unit III debris-flow deposit.

Unit III in both Holes 941A and 941B contains planktonic and bathyal benthic foraminifers, iron-stained foraminifer tests, pteropods, ostracode shells, calcareous echinoid spines and shell fragments, fish scales and bones, wood, and mica. Unit III has two distinct planktonic foraminifer assemblages: (1) glacial-aged material containing *P. obliquiloculata*, suggesting a sediment age older than 40 ka but younger than 85 ka, and (2) interglacial material containing relatively high abundances of *G. menardii*, *G. tumida*, and *G. tumida flexuosa*. The presence of *G. tumida flexuosa* shows that the age of the original source of the foraminifers must have been a recent interglacial (oxygen isotopic Stages 5 to 11), and the relatively high abundances of *G. tumida flexuosa* suggest oxygen isotopic Stage 5 (Ericson X Zone). It is not possible to determine if there are glacial-aged foraminifers mixed in this second assemblage. By correlating between Holes 941A and 941B, which are 500 m apart, Unit III was subdivided into two distinct and alternating "biounits" (Fig. 26). These biounits appear to represent alternating glacial and interglacial sediment sources for the debris-flow Unit III.

Unit IV has been preliminarily defined as Ericson Y Zone (<40 ka) due to the absence of *G. menardii*, *G. tumida*, and *P. obliquiloculata*. However, Unit IV could be an older glacial section, as Site 941 represents an incomplete stratigraphic section due to the debris-flow deposit, and age- diagnostic taxa are lacking in Unit IV.

Unit III, the debris flow, is directly overlain by Holocene sediment and is therefore likely of early Holocene or latest Pleistocene age.

Benthic Foraminifers

Abyssal benthic foraminifers occur in low abundances in Unit II in Hole 941A, whereas bathyal benthic foraminifers occur in moderate abundances in Units I and II in Hole 941B. Unit III in both Holes 941A and 941B contains high abundances of bathyal benthic foraminifers (most abundant species are *Bolivina* sp., *Bulimina* sp., and *Miliolinella* sp.) and low abundances of abyssal benthic foraminifers (*Pyrgo* sp.), suggesting reworking. Unit IV is nearly barren of benthic foraminifers.

Siliceous Microfossils

The siliceous microfossil assemblage of the mud-line sample of Hole 941A includes rare marine diatoms (e.g., the solution-resistant species *Coscinodiscus nodulifer*), freshwater diatoms (*Melosira granulata*), and a few specimens of silicoflagellates (*Dictyocha* sp.).

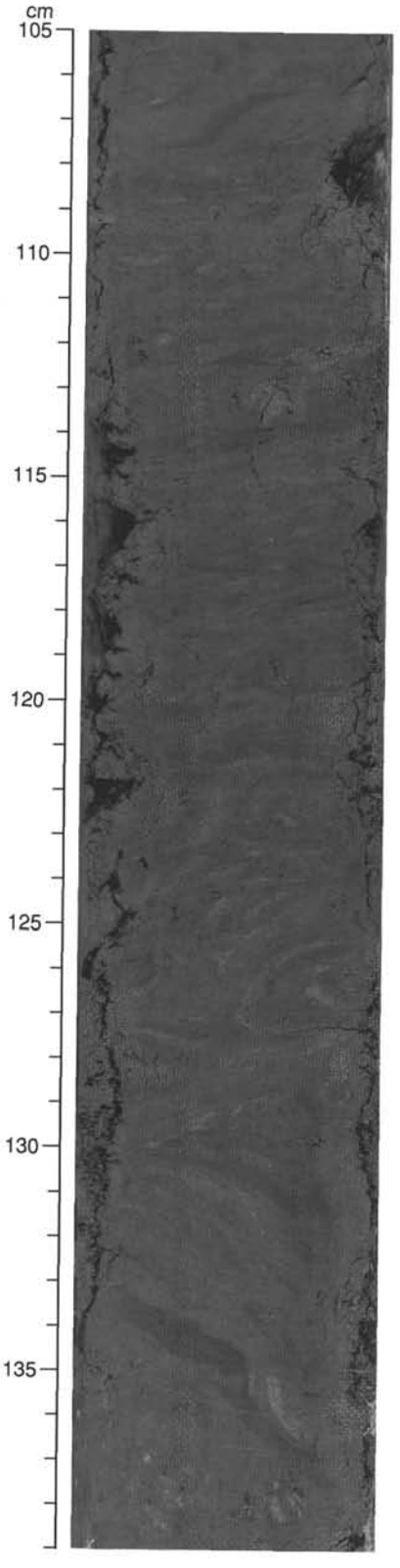

Figure 22. Folded and deformed beds and clasts in Unit III (155-941A-9X-2, 105–139 cm). Deformed clasts of silt and fine sand occur between 108 and 114 cm, and below 123 cm (lightest color shades). In this interval, the deformed and folded beds and larger clasts form "wood-grain" patterns because of "biscuit" formation by drilling disturbance.

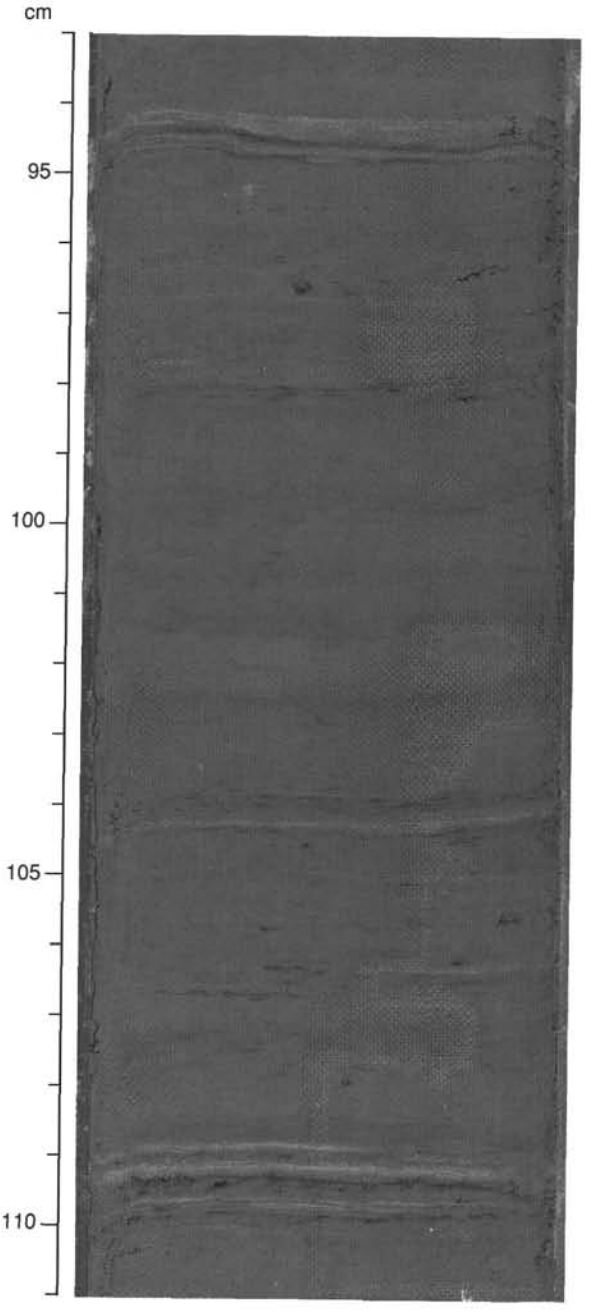

Figure 23. Parallel- and cross-lamination in thin silt laminae in Unit IV (155-941A-18X-6, 93–111 cm).

The pre-Holocene section of Hole 941A is barren of diatoms (Table 4). Siliceous sponge spicules have a scattered occurrence throughout Hole 941A.

Palynology

Eight samples were examined from Hole 941A (Table 5). Pollen and spore assemblages were obtained from clay, silty clays and silt (Units III and IV) between 5.29 mbsf and 176.84 mbsf (Fig. 27). The assemblages have low to moderate abundance of spores and pollen, and contain Cyperaceae, Euphorbiaceae, and stephanocolpate and tricolpate (TC) types, with Cyatheaceae, trilete spores, and monolete spores. Poor to moderate preservation of pollen and spores is characteristic of these assemblages, suggesting that reworked pollen and spores from older, previously deposited sediment may be a signifi-

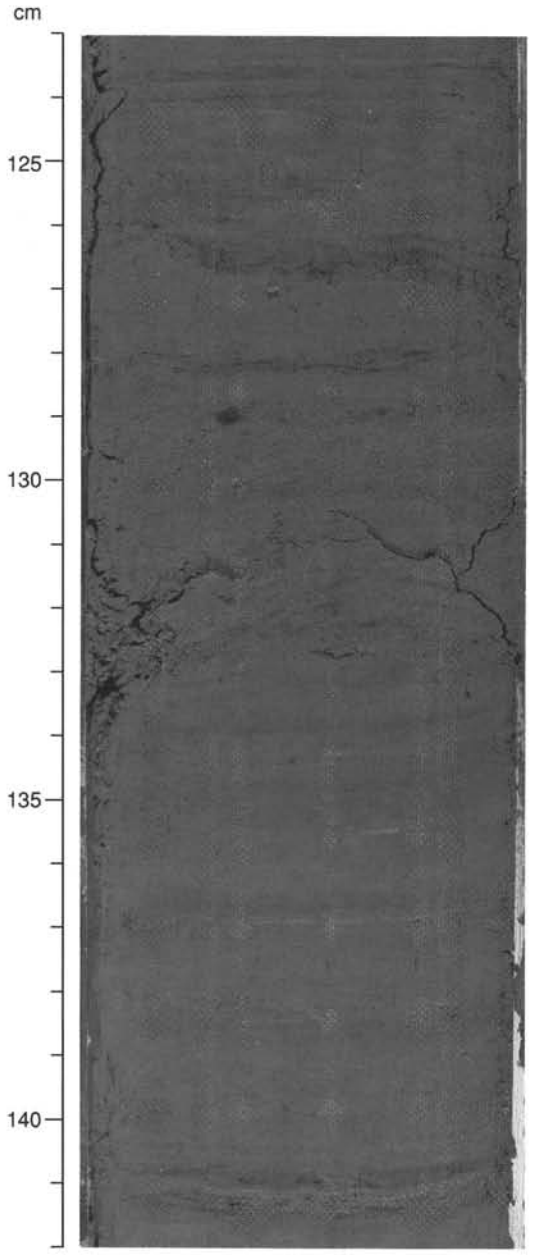

Figure 24. Parallel- and cross-lamination in normally graded silt beds and silt laminae in Unit IV (155-941A-16X-3, 123–142 cm).

cant element of the total palynomorph assemblage. Wood particles were observed in all sample slides in low to moderate abundance (Table 5). Dinoflagellates are present in very low abundance at 93.59 and 187.15 mbsf.

Stratigraphic Summary

The boundary between Ericson Zones Z and Y cannot unequivocally be defined at Site 941, as abundant *G. tumida* is found down to the lithostratigraphic boundary between Units II and III (the debris-flow deposit) at 5.3 mbsf. The age of Unit III can be constrained to older than 9 ka. Unit IV has been defined as Y Zone (younger than 40 ka) due to the absence of *G. menardii*, *G. tumida*, and *P. obliquiloculata*, but it might be older.

PALEOMAGNETISM

Remanence Studies

Measurements were made with the pass-through cryogenic magnetometer on the archive halves of all APC and XCB cores. Tensor tool orientations were obtained for Cores 941A-3H through -7H and 941B-3H through -9H. In general, only single sections of the cores from Unit III (debris flow) were measured. This is because the characteristic remanence directions within the debris flow were highly variable, with rapidly changing inclinations over boundaries between blocks or fold structures. XCB cores from the levee system beneath the debris flow generally had a persistent drill stem overprint, and so their remanence directions are also of questionable significance.

Azimuthally uncorrected declinations, inclinations, and remanence intensities, after AF demagnetization to 20 mT, are shown for the Hole 941A and Hole 941B archive halves from Unit I (calcareous clay) and Unit II (hemipelagic muds) (Figs. 28 and 29). Short wavelength oscillations appear in all three remanence parameters for both holes, but they are best developed in the inclination and intensity data. Peaks in positive inclination and remanence intensity have been numbered on each figure.

Magnetic Susceptibility Studies

Whole-core magnetic susceptibility was measured on all cores from Site 941. Discrete-sample measurements were performed only on samples from Hole 941A. The results from Hole 941A are used to represent the site in Figure 30.

The highest susceptibility values are found within Unit IV; the lowest values are within Unit I. The susceptibility data in Unit III show large variations that may reflect debris-flow packets. The whole-core susceptibility signal between about 7 and 25 mbsf has low variability that contrasts with the high variability in susceptibility from about 25 to 44 mbsf.

ORGANIC GEOCHEMISTRY

Volatile Hydrocarbons

Headspace methane concentrations increase rapidly below the sediment surface to a maximum value of 34,940 ppm at 11.56 mbsf (Table 6; Fig. 31). Methane concentrations remain fairly constant below this depth, ranging from 4,600 ppm to 10,400 ppm. Vacutainer methane values are considerably higher than headspace concentrations (Fig. 31), ranging from 61,000 ppm at 52.58 mbsf to 453,000 ppm at 25.78 mbsf. Higher molecular weight hydrocarbons were not present, indicating a predominantly biogenic methane source at Site 941.

Carbon, Nitrogen, and Sulfur Concentrations

Carbonate, calculated as $CaCO_3$, contents are high at 0.18 mbsf (32%) and 0.53 mbsf (79%) (Table 7; Fig. 32) and generally remain low (<3%) in the rest of Hole 941A. Slightly elevated carbonate values (>5%) found at 3.29 mbsf, 31.16 mbsf, and 120.16 mbsf correspond to layers or clasts of gray clay. TOC concentrations are low (0.3%) in the foraminifer-rich clay at 0.18 mbsf and extremely low (0.02%) in the foraminifer-rich sand at 0.53 mbsf. In the rest of the hole, TOC concentrations range from 0.6% to 0.85% with low values (<0.6%) observed in silt beds. In general, TOC concentrations throughout most of Hole 941A are lower than at previous sites.

Total nitrogen concentrations range between 0.05% and 0.10%. The lowest TN concentrations (<0.05%) were measured in the foraminifer-rich sand at 0.53 mbsf and in the silt beds below 140 mbsf. Overall, total sulfur concentrations are low (<0.3%) but, as at previous sites, high values (>1.4%) were measured below Unit I at 3.29

Table 2. Relative peak intensities of the main minerals in samples of silty clay from Hole 941A.

Core, section, interval (cm)	Depth (mbsf)	Relative intensity of primary peaks						
		Smectite	Mica + Illite	Kaolinite	Quartz	Plagioclase	K-feldspar	Augite
155-941A-								
1H-3, 137–138	4.37	12.5	14.2	11.2	100.0	12.5	*	4.5
2H-7, 125–126	14.36	10.5	18.7	13.3	100.0	10.9	*	3.5
3H-5, 70–71	21.50	10.0	18.7	12.8	100.0	11.4	*	4.6
4H-6, 106–107	32.80	14.0	15.7	15.3	100.0	13.1	*	4.2
5H-1, 120–121	35.00	6.5	13.6	11.4	100.0	8.2	*	3.5
6H-6, 137–138	50.95	10.5	21.2	9.5	100.0	8.5	9.5	2.4
7H-5, 110–111	57.68	15.9	23.2	14.1	100.0	10.5	*	4.0
8X-2, 110–111	64.80	7.5	23.1	14.1	100.0	10.1	*	3.5
9X-2, 90–91	74.20	11.9	19.9	13.6	100.0	11.4	6.8	3.3
10X-1, 100–101	82.30	9.4	17.2	12.1	100.0	8.4	*	3.0
14X-2, 107–108	122.57	7.1	15.2	13.1	100.0	7.7	*	2.7
15X-4, 90–91	135.10	9.5	18.4	12.4	100.0	7.5	6.3	2.6
16X-1, 44–45	139.74	8.4	21.1	12.0	100.0	8.5	4.7	2.4
17X-3, 56–57	152.46	7.4	22.0	15.7	100.0	9.0	*	3.2
18X-4, 134–135	164.44	12.4	26.4	12.6	100.0	8.0	4.1	3.4
19X-5, 47–48	174.67	14.6	23.9	15.8	100.0	9.6	15.8	2.7

Notes: See "Lithostratigraphy" section in the "Explanatory Notes" chapter, this volume, for XRD methods. * = non-detection.

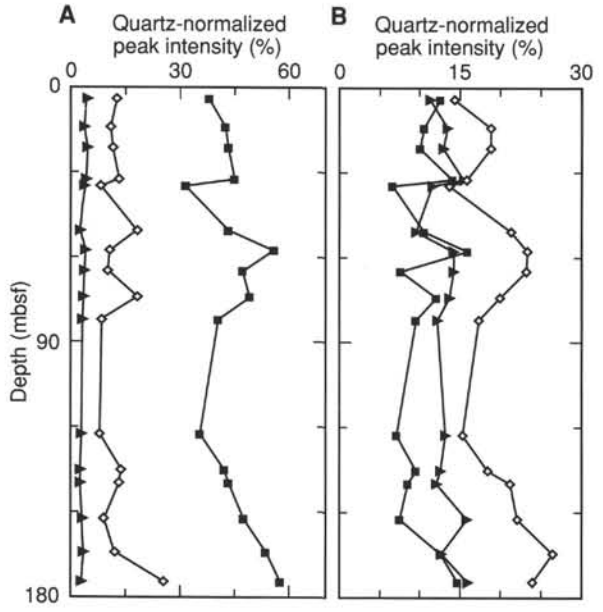

Figure 25. XRD mineralogy. **A.** Downhole variation in the relative peak intensities of the main mineral groups in Site 941 sediment. Squares = clay minerals + mica; diamonds = feldspar; triangles = augite. **B.** Downhole variation in the relative peak intensities of clay minerals and micas. See text for discussion. Squares = smectite; diamonds = mica + illite; triangles = kaolinite.

and 4.24 mbsf. A moderately high TS content (0.7%) was also measured at 111.46 mbsf. The [C/N]a ratios in the top 0.5 mbsf are less than 5, whereas they range from 8 to 12 in the rest of the hole.

INORGANIC GEOCHEMISTRY

Interstitial Water Analysis

Interstitial-water analyses were performed on nine sediment samples at Hole 941A. Samples were taken approximately every 10 m for the upper 37 mbsf and approximately every 30 m thereafter to a depth of 173.60 mbsf (Table 8; Fig. 33).

Salinities of the water samples range from 29.5 to 34.0 (Fig. 33A). Between 2.95 and 13.06 mbsf, salinity decreases from 34.0 to 32.0, and is then constant at 32.0 to 65.10 mbsf. At 112.27 mbsf, the salinity decreases to 29.5, which is considerably below seawater salinity. In the two lowermost samples, salinity increases again to 33.0.

Chloride concentrations range from 496 to 563 mM. Concentrations increase in the upper 30 mbsf, from 552 mM at 2.95 mbsf to 563 mM at 31.69 and 36.72 mbsf (Fig. 33B). From 36.72 to 112.27 mbsf, the chloride concentration declines to 496 mM, well below seawater chlorinity, then increases to 556 mM at 145.20 mbsf and to 566 mM at 173.60 mbsf.

Pore-water pH values are relatively high in the uppermost sample, 8.11 at 2.95 mbsf (Fig. 33C). The values decrease to 7.65 at 13.06 mbsf and remain at about 7.5 downhole, with the exception of a value of 7.09 at 145.20 mbsf.

Alkalinity values fall into a fairly narrow range, from 14.51 to 8.64 mM. These values tend to decrease in the upper 36.72 mbsf, then remain near 10 mM downhole (Fig. 33D).

Magnesium and calcium concentrations decrease in the upper 13.06 mbsf, from presumably seawater values at the sediment surface to 37.7 mM magnesium and 4.5 mM calcium at 13.06 mbsf (Fig. 33E and 33F), and remain near those values down to 65.10 mbsf. Concentrations decrease further, to 29.5 mM magnesium and 4.2 mM calcium at 112.27 mbsf, then increase again, to about 42 mM magnesium and 5.5 mM calcium in the two lowermost samples.

Pore-water sulfate concentrations decrease quickly in the upper part of the hole, from 11.3 mM at 2.95 mbsf to zero at 13.06 mbsf (Fig. 33G). Below 13.06 mbsf, sulfate concentrations generally remain at or near zero. Values above zero were recorded, however, at 65.10 and 173.60 mbsf (2.5 and 3.1 mM). High methane concentrations measured at these same depths suggest that the measured sulfate value represents a sampling artifact.

Ammonium concentrations increase steadily with depth, from 1.1 mM at 2.95 mbsf to 8.5 mM at 65.10 mbsf (Fig. 33H). Below 65.10 mbsf, the ammonium concentration is more constant, varying between 8.5 and 6.5 mM.

Pore-water phosphate concentrations are very high in the uppermost sample, 199 µM at 2.95 mbsf. Concentrations decrease to 10.4 µM at 13.06 mbsf and generally remain at about 10 µM downhole (Fig. 33I).

Dissolved silica concentrations range from 132 to 357 µM (Fig. 33J). Concentrations increase from 138 µM at 2.95 mbsf to 294 µM at 22.25 mbsf. Thereafter, values generally remain between 300 and 350 µM.

The pore-water potassium concentration is 12.2 at 2.95 mbsf, then decreases to 9.1 mM at 13.06 mbsf and remains between 9.1 and 9.3 mM to 31.69 mbsf (Fig. 33K). Concentration of potassium increases to 13.0 at 36.72 mbsf, and then decreases again to between 6 and 7 mM for the remainder of the hole.

Table 3. Calcareous nannofossil and siliceous microfossil abundance data for Hole 941A.

Core, section, interval (cm)	Top interval (mbsf)	Bottom interval (mbsf)	Calcareous nannofossils			Diatoms				Ericson Zone (inferred from foraminifers)	Age (inferred from foraminifers)
			Abundance	Preservation	Zone	Marine	Fresh water	Sponge spicules	Radiolarians		
155-941A-											
1H-1, Ml	0.00		a	g	CN15b	r	vr	c	vr	Z	Holocene
1H-1, 7–8	0.07	0.08	a	g		r	vr	c	b	Z	Holocene
1H-1, 23–25	0.23	0.25	a	g		vr	b	r	b	Z	Holocene
1H-1, 33–34	0.33	0.34	f	g		tr	b	r	b	Z	Holocene
1H-1, 42–43	0.42	0.43	a	g		b	b	r	b	Z	Holocene
1H-CC, 20–21	5.29	5.30	vr	—		b	b	b	b	Z	Holocene
2H-CC, 32–33	15.50	15.51	vr	—		b	b	b	b	RW	late Pleist.
3H-5, 27	21.07		b	—		b	b	b	b	RW	late Pleist.
3H-6, 70	23.00		b	—		b	b	b	b	RW	late Pleist.
3H-CC, 20–21	24.84	24.85	r	—		b	b	b	b	RW	late Pleist.
4H-2, 34	26.12		f	m		b	b	f	b	RW	late Pleist.
4H-5, 62	30.86		a	m		b	b	c	b	RW	late Pleist.
4H-5, 99	31.23		a	g		b	b	b	b	RW	late Pleist.
4H-5, 117	31.41		a	m		b	b	b	b	RW	late Pleist.
4H-5, 122	31.46		f	m	RW (Tertiary)	b	b	b	b	RW	late Pleist.
4H-6, 140	33.14		a	m	RW (Tertiary)	b	b	b	b	RW	late Pleist.
4H-6, 144	33.18		f	m	RW (Tertiary)	b	b	b	b	RW	late Pleist.
4H-7, 15.5	33.40		b			b	b	b	b	RW	late Pleist.
4H-7, 17.5	33.42		a	m	RW (Tertiary)	b	b	b	b	RW	late Pleist.
4H-7, 24	33.48		r	p		b	b	b	b	RW	late Pleist.
4H-7, 25	34.48		a	g	RW (Tertiary)						
4H-7, 43	52.48		a	g	RW (Tertiary)						
5H-2, 127	35.07		a	g	RW (Tertiary)						
5H-4, 128	37.82		a	g	RW (Tertiary)						
5H-4, 11	36.65		vr	p	CN15						
5H-CC, 91–92	42.56	42.57	r	—		b	b	vr	b	RW	late Pleist.
6H-CC, 34–35	53.77	53.78	tr	—		b	b	b	b	RW	late Pleist.
7H-CC, 79–80	59.14	59.15	tr	—		b	b	b	b	RW	late Pleist.
8X-CC, 19–20	66.27	66.28	vr	—		b	b	b	b	RW	late Pleist.
9X-CC, 12–13	74.82	74.83	b	—		b	b	b	b	RW	late Pleist.
10X-CC, 20–21	83.00	83.01	vr	—		b	b	b	b	RW	late Pleist.
13X-CC, 14–15	115.38	115.39	vr	—		b	b	b	b	RW	late Pleist.
14X-1, 17–18	120.17	120.18	vr	—		b	b	b	b	RW	late Pleist.
14X-CC, 14–15	124.07	124.08	r	—		b	b	b	b	RW	late Pleist.
15X-CC, 27–28	139.45	139.46	tr	—		b	b	b	b	Y (?)	late Pleist.
17X-CC, 14–15	156.46	156.47	tr	—		b	b	b	b	Y (?)	late Pleist.
18X-CC, 15–16	167.67	167.68	tr	—		b	b	b	b	Y (?)	late Pleist.
19X-CC, 27–28	176.84	176.85	b	—		b	b	b	b	Y (?)	late Pleist.

Dissolved sodium concentrations decrease slightly in the uppermost part of the hole, from 477 mM at 2.95 mbsf to 468 mM at 36.72 mbsf (Fig. 33L). At 112.27 mbsf, the concentration decreases to an anomalously low value of 425 mM. Below that depth, the concentration increases to 470 mM near the bottom of the hole.

Dissolved iron concentrations are variable (Fig. 33M) and increase sharply in the three uppermost samples, to 99.5 µM at 22.25 mbsf. Below this depth, the concentrations vary between 11.4 and 86.4 µM, with no clear trend downhole.

Manganese concentrations increase from 2.8 µM at 2.95 mbsf to 8.0 µM at 31.69 mbsf. Below this depth, the concentrations decrease to 4.0 µM at 36.72 mbsf, and remain below 5 µM downhole.

There are several unusual diagenetic features at Site 941. One is the low chloride concentration (496 mM) at 112.27 mbsf. Relatively low salinity and magnesium and sodium concentrations also were measured at this depth. The low dissolved solid concentrations suggest pore-water dilution, probably through melting of a previously precipitated clathrate. No sedimentological evidence for a clathrate was observed in nearby sediment, though this may be due to poor recovery in the cores above and below this sample. As at several previous sites, the low chloride value is from within a debris-flow unit.

A second unusual feature is the observed large (up to several centimeters), sometimes euhedral crystals of what are presumed to be ikaite (941A-1H-3, 7–18 and 88–94 cm). These crystals were initially a yellow-brown color, but turned a milky yellow several hours after the core was split, and eventually began to disintegrate. A freeze-dried sample prepared for X-ray diffraction (XRD) analysis turned to a white powder, with considerable weight loss. XRD analyses of both the freeze-dried sample and a wet-ground smear slide of the crystals showed only calcite. A small siderite (verified by XRD) nodule (5 cm) was also recovered (Sample 941B-11H-CC, 50–55 cm). Siderite also was found in a tan mud layer (941B-3H-5, 42–43 cm). Finally an approximately 5-cm nodule of dense, crystalline vivianite was found (Sample 941A-4H-4, 91–92 cm). The morphology is distinctly different from the millimeter-sized, microcrystalline nodules commonly found in the sediment.

Sediment Geochemistry

Three mud samples from the debris-flow deposit and one from lithostratigraphic Unit IV were analyzed for major- and trace-element geochemistry (Tables 9 and 10). Compositions and element ratios are similar to those at previous sites. SiO_2 ranges from 59 to 62 wt%, Al_2O_3 between 22 and 23 wt%, and CaO abundances between 0.8 and 0.9 wt%, indicating a dominantly silicate mineralogy.

PHYSICAL PROPERTIES

Index Properties

Index properties were measured for samples from lithologic Units II through IV in Holes 941A and 941B (Table 11). Water content decreases with depth from 61% near the top of Unit II to 26% at 174.9 mbsf (Fig. 34). Close to the base of Unit II, at 4.90 mbsf in Hole 941A, water content is reduced to 53%. Variable water content and a downhole decrease from approximately 37% to 27% characterize Unit III (5.30–129.70 mbsf, Hole 941A). Within Unit III, water content is unusually high at 48.34, 63.15, and 75.41 mbsf; however, the values at these depths may be drilling artifacts. Two of the samples (Samples 941A-11H-1, 31–33 cm, and 941B-8X-1, 85–87 cm) were probably affected by core top disturbance. The third sample (Sample 941B-6H-3, 74–76 cm) was taken 10 cm from an interval disturbed

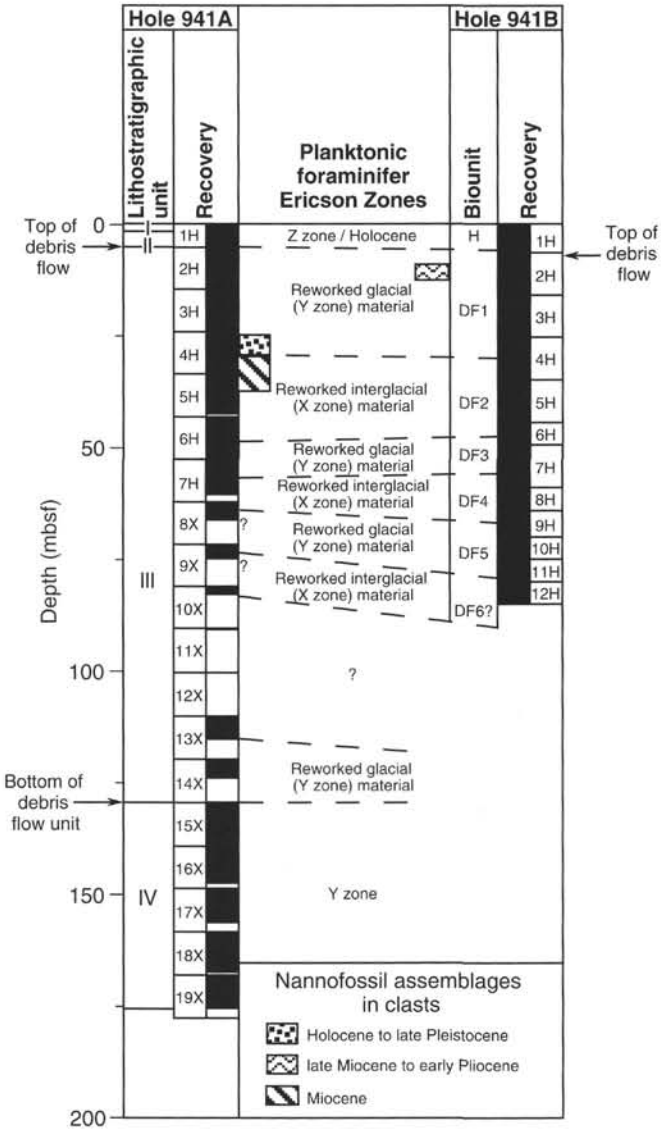

Figure 26. Correlation of the planktonic foraminifer assemblages found in the debris-flow deposit of Holes 941A and 941B.

by core liner collapse. Unit IV (129.70–177.92 mbsf) displays a more uniform downhole decrease in water content, with values decreasing from 28% to 26%. A slight increase in water content, 1.5%, occurs between the bottom of Core 941A-16X and the top of Core 941A-17X. Because this change occurs at the break between cores, it is not clear whether it represents a change in the sediment, or coring-induced change as seen in XCB cores at previous sites.

Porosity and wet-bulk-density profiles display variation that matches the water content variation (Fig. 34). In general, porosity decreases downhole from 81% to 48%, and wet-bulk density increases from 1.39 to 1.97 g/cm^3. Grain density at the site averages 2.76 g/cm^3, and mostly varies between 2.7 and 2.8 g/cm^3.

The GRAPE bulk-density profile is unusual in that the GRAPE densities for the upper 5 m of Hole 941A are 0.05 to 0.25 g/cm^3 higher than the discrete-sample wet-bulk densities (Fig. 34). The origin of this discrepancy is uncertain. Between 5 and 65 mbsf, the GRAPE and discrete-sample data progressively diverge as the GRAPE densities are reduced by gas-induced expansion. Below 65 mbsf, the difference between GRAPE and discrete-sample wet-bulk density varies between 0.30 and 0.40 g/cm^3.

The primary features of the index property profiles at Site 941 are similar to those at previous Amazon Fan sites. The mass transport deposit of Unit III is characterized by low and variable water content, and the silty clay levee deposits of Unit IV display more uniform downhole trends. However, in contrast to Sites 931 and 933, there are not significant increases in water content and porosity and a decrease in wet-bulk density at the top of the Unit IV levee deposit. The explanation for the apparent normal consolidation of the levee deposits is not presently known, and its determination is made difficult by the poor recovery in the lower part of Unit III.

Compressional-wave Velocity

Pervasive microfractures resulting from gas expansion restricted velocity measurements to sub-bottom depths less than 5.9 mbsf. Four pairs of longitudinal and transverse velocity measurements were made with the DSV between 1.14 and 4.90 mbsf in Hole 941A. Over this interval the longitudinal velocity ranges from 1490 to 1522 m/s and averages 1502 m/s. The average velocity anisotropy is 1.6%. Transverse velocities were obtained by the PWL for the intervals 0–4.40 mbsf in Hole 941A and 0–5.90 mbsf in Hole 941B. Average velocities for these two intervals are 1492 and 1502 m/s, respectively.

Shear Strength

Measurements of undrained shear strength were made using the motorized shear vane on all cores from Holes 941A and 941B (Table 12). Compressive strengths were determined with a pocket penetrometer and used to estimate undrained shear strength below 44 mbsf in Hole 941A and 54 mbsf in Hole 941B.

In contrast to previous Amazon Fan sites, the shear-strength profile at Site 941 displays highly variable strength at shallow depths (Fig. 35). The overall trend in Hole 941B and the upper part of Hole 941A is an increase from 4.6 kPa near the top of Unit II to 145.0 kPa at approximately 75 mbsf. The extent of the variability is exemplified by four samples in this interval (Samples 941A-2H, 54–56 cm; -2H-8, 37–39 cm; -3H-2, 121–123 cm; and -4H-4, 104–106 cm) that have shear strengths significantly higher than those of adjacent sediment. These samples are also characterized by low water content and high bulk density, suggesting that they are resedimented, previously consolidated clasts. The scatter in the strength data increases below 63 mbsf. Below the maxima at 75 mbsf, there are no consistent trends with depth within Unit III. The boundary between Units III and IV is marked by reductions in the magnitude and variability in strength. In Unit IV, there is a general downhole increase in shear strength, from approximately 50 to 65 kPa.

The residual to peak undrained shear strength ratio is characterized by considerable scatter. The ratio decreases downhole from about 0.75 just below the seafloor to 0.65 at 45 mbsf. Below 45 mbsf, there is little change in the ratio with depth, and most of the values cluster about 0.60.

As at previous Amazon Fan sites, some of the variability in shear strength may reflect consequences of coring disturbance. This disturbance is indicated by the step-like strength increase within individual cores. Site 941 differs from previous sites in that the step-like changes occur within individual APC cores as well as XCB cores. This effect is most noticeable in Cores 941A-8X and -18X and Cores 941B-4H, -7H, -8H, and -11H (Table 12).

Resistivity

Longitudinal and transverse resistivity were determined for cores from Holes 941A and 941B (Table 13). Longitudinal resistivity displays a downhole increase that generally parallels the downhole decrease in porosity, but with greater variability (Fig. 36). Resistivity increases from approximately 0.20 Ωm near the seafloor to 0.40 Ωm at 84 mbsf. Below the recovery gap between 83 and 110 mbsf in Hole

Table 4. Foraminifer abundance data for Holes 941A and 941B.

Core, section, interval (cm)	Top interval (mbsf)	Bottom interval (mbsf)	*Globorotalia menardii*	*Globorotalia tumida*	*Globorotalia tumida flexuosa*	*Pulleniatina obliquiloculata*	*Globigerinoides ruber* (white)	*Globigerinoides ruber* (pink)	*Globorotalia hexagonus*	*Neogloboquadrina dutertrei*	*Globorotalia trilobus trilobus*	*Globorotalia inflata*	*Globorotalia truncatulinoides*	*Globigerina bulloides*	*Globigerinoides trilobus sacculifer*	*Globorotalia fimbriata*	*Bolliella adamsi*	*Hastigerinella digitata*	*Globigerina calida calida*	*Globorotalia crassaformis hessi*	*Globorotalia crassaformis viola*	*Globorotalia tosaensis*	*Globorotalia crassaformis crassaformis*	Other planktonic foraminifers	Vivianite nodules	Overall foraminifer abundance	Preservation	Abundance of bathyal benthic foraminifers	Abundance of abyssal benthic foraminifers	Comments	Ericson Zone	Age
155-941A-																																
1H-Ml, 0–0	0.00	0.00	F	R	B	R	F	R	B	F	C	B	B	B	C	R	B	B	R	B	B	B	B	B	B	A	G	B	B	PT	Z	Holocene
1H-1, 7–8	0.07	0.08	C	F	B	R	F	R	B	C	C	B	B	B	F	R	B	B	B	B	B	B	B	B	B	A	G	B	B		Z	Holocene
1H-1, 33–34	0.33	0.34	C	F	B	F	C	F	B	F	C	B	B	B	F	R	B	B	B	B	B	B	B	B	B	A	G	B	B	M, SP	Z	Holocene
1H-1, 42–43	0.42	0.43	F	F	B	F	C	F	B	F	C	B	B	B	C	B	B	B	B	B	B	B	B	B	B	A	G	B	B	SP	Z	Holocene
1H-1, 50–51	0.5	0.51	C	C	B	F	F	F	B	C	C	B	B	B	C	R	B	B	B	B	B	B	B	B	B	A	G	B	B	PT	Z	Holocene
1H-1, 90–92	0.9	0.92	F	C	B	F	F	F	B	C	C	B	B	B	F	R	B	B	R	B	B	B	B	B	B	A	G	B	B		Z	Holocene
1H-1, 143–148	1.43	1.48	C	F	B	C	F	F	B	C	C	B	F	B	F	R	B	B	B	B	B	B	B	B	B	A	G	B	R	PT	Z	Holocene
1H-3, 63–68	3.63	3.68	F	F	B	F	C	F	B	C	C	B	B	B	F	B	B	B	B	B	B	B	B	B	R	B	F	G	B	R	BN	Z	Holocene
1H-CC, 6–20	5.15	5.29	F	C	B	F	F	B	B	C	C	B	F	B	R	R	B	B	B	B	B	B	B	B	B	B	C	G	R	R	RN, ES, SP	Z	Holocene
2H-CC, 18–32	15.36	15.50	B	B	B	F	F	R	B	C	C	B	C	B	C	B	B	B	B	B	B	B	B	B	B	B	C	G	A	B	IS, BN, SF, ES, ESh, PT	RW (Y)	late Pleist.
3H-CC, 6–20	24.70	24.84	B	B	B	F	F	B	B	C	C	B	C	B	C	B	B	B	B	B	B	B	B	B	B	C	C	P	A	B	ES, ESh, OS, FS, PT, SF	RW (Y)	late Pleist.
4H-CC, 22–36	34.02	34.16	F	F	R	F	F	B	B	C	C	B	F	B	F	B	B	B	B	B	B	B	B	B	B	C	C	G	C	B	IS, OS, ES, BN	RW (Y+X)	late Pleist.
5H-CC, 77–91	42.32	42.56	B	F	R	F	R	B	B	C	C	B	F	B	F	B	B	B	B	B	B	B	B	B	B	C	C	M	A	B	ES, ESh, PT, BN	RW (Y+X)	late Pleist.
6H-CC, 20–34	53.63	53.77	B	B	B	R	C	B	B	C	C	B	F	B	F	B	B	B	B	B	B	B	B	B	B	F	C	M	A	R	ES, ESh, OS, PT, BN	RW (Y)	late Pleist.
7H-CC, 65–79	58.20	58.34	R	B	R	F	F	B	B	C	C	B	F	B	F	B	B	B	B	B	B	B	B	B	B	C	A	M	A	R	ES, ESh, PT, OS, FS, BN	RW (Y+X)	late Pleist.
8H-CC, 5–19	66.13	66.27	R	R	B	F	F	B	B	C	C	B	F	B	F	B	B	B	B	B	B	B	B	B	B	C	C	M	A	B	ES, ESh, BN, PT, S	RW (Y+X)	late Pleist.
9H-CC, 0–13	74.68	74.82	B	B	B	R	R	B	B	C	C	B	R	B	C	B	B	B	B	B	B	B	B	B	B	F	F	M	C	R	W, M	RW (Y)	late Pleist.
10H-CC, 6–20	82.86	83.00	R	R	R	F	C	B	B	C	C	R	F	B	F	B	B	B	B	B	B	B	R	B	F	F	M	A	R	SF, IS, SP, BN, S	RW (Y+X)	late Pleist.
13X-CC, 0–14	115.24	115.38	B	B	B	R	R	B	B	R	B	B	R	B	B	B	B	B	B	B	B	B	B	B	F	R	M	A	F	SP, BN, IS, OS	RW (Y)	late Pleist.
14X-CC, 0–14	123.93	124.07	B	B	B	C	C	B	B	F	C	B	F	B	F	B	B	B	B	B	B	B	B	B	F	A	M	C	B	S, BN, IS, SF, S	RW (Y)	late Pleist.
15X-CC, 13–27	139.31	139.45	B	B	B	B	C	B	B	F	C	B	F	B	C	B	B	B	B	B	B	B	B	R	C	C	G	B	B	M	Y (?)	late Pleist.
16X-CC, 52–66	147.67	147.81	B	B	B	B	C	R	B	C	C	B	B	B	F	B	B	B	B	R	B	B	B	B	C	C	G	R	B	M, RN	Y (?)	late Pleist.
17X-CC, 0–14	156.32	156.46	B	B	B	B	F	B	B	F	C	B	F	B	C	B	B	B	B	B	B	B	R	B	C	F	G	B	B	M	Y (?)	late Pleist.
18X-CC, 1–15	167.53	167.67	B	B	B	B	A	R	B	C	C	B	F	B	C	B	B	B	B	F	B	B	R	B	F	C	G	B	B		Y (?)	late Pleist.
19X-CC, 13–27	176.70	176.84	B	B	B	B	C	B	B	C	A	B	B	B	R	B	B	B	B	B	B	B	B	B	A	R	G	B	B	M	Y (?)	late Pleist.
155-941B-																																
1H-Ml, 0–0	0.00	0.00	C	F	B	R	A	F	B	F	C	B	F	B	C	F	B	B	R	R	B	B	B	B	B	A	G	F	B	PT	Z	Holocene
1H-CC, 5–19	6.45	6.59	R	F	B	F	A	R	B	F	C	B	F	B	C	R	B	B	B	R	B	B	B	B	B	A	G	R	B	SF,SP,BN,PT,IS	Z	Holocene
2H-CC, 22–36	16.77	16.91	B	B	B	B	C	B	B	F	C	B	C	B	C	B	B	B	B	R	B	B	B	B	B	C	M	B	B	SP,IS, BN, SF, PT	RW (Y)	late Pleist.
3H-CC, 68–82	25.14	25.28	R	B	B	F	C	B	R	F	C	B	F	B	F	B	B	B	B	R	B	B	B	B	F	F	M	A	B	IS,SP,BN,OS,PT	RW (Y)	late Pleist.
4H-CC, 34–40	34.58	34.72	B	B	B	B	C	B	R	F	B	B	C	B	A	B	B	B	B	B	B	B	B	B	B	A	M	C	B	SP,IS,BN,PT	RW (Y+X)	late Pleist.
5H-CC, 115–129	43.49	43.63	B	B	B	B	C	B	B	C	C	B	F	F	F	B	B	B	B	R	B	B	B	B	B	C	P	A	B	IS,BN,SP,SF,PT,S	RW (Y+X)	late Pleist.
6H-CC, 26–40	51.67	51.81	B	B	B	F	C	R	B	C	C	R	F	B	F	B	B	B	B	B	B	B	B	B	B	C	P	A	B	SP,IS,BN,PT,W,OS	RW (Y)	late Pleist.
7H-CC, 71–85	59.68	59.82	R	F	F	F	C	B	B	C	C	R	C	F	B	B	B	B	B	R	B	B	B	B	R	A	M	A	R	SP,IS,BN	RW (Y+X)	late Pleist.
8H-CC, 55–69	65.20	65.34	B	B	B	B	F	C	B	C	C	B	F	B	F	B	B	B	B	B	B	B	B	B	R	C	M	C	F	S,SP,BN,PT,IS	RW (Y+X)	late Pleist.
9H-CC, 15–29	69.53	69.57	B	R	B	B	C	B	B	C	F	B	C	B	B	B	B	B	B	B	B	B	B	B	R	F	M	C	B	SP,BN,S,PT	RW (Y)	late Pleist.
10H-CC, 37–76	75.57	75.71	B	B	B	C	C	B	B	C	F	B	B	B	F	B	B	B	B	B	B	B	B	B	R	F	M	A	B	SP,BN,OS	RW (Y+X)	late Pleist.
11X-CC, 30–54	80.90	81.04	B	B	B	F	C	R	B	C	C	B	F	B	B	B	B	B	B	B	B	B	B	B	R	C	M	C	B	SP,BN,IS	RW (Y)	late Pleist.
12X-CC, 66–80	86.16	86.30	B	B	B	F	C	R	B	C	C	B	F	B	F	B	B	B	B	B	B	B	B	B	F	C	P	C	B	SP,BN,IS	RW (Y)	late Pleist.

Notes: Key to Comments section: Sediment composition: PT = pteropods, S = sand, M = mica, BN = black nodules, RN = red nodules; indicators of reworking: SF = shell fragments, W = wood fragments, OS = ostracod shells, ES = echinoid spines, ESh = echinoid shells, FS = fish scales, SP = sponge spicules or spines, IS = iron-stained foraminifers. Note also the occurrence of bathyal benthic foraminifers.

Table 5. Spores and pollen data for Hole 941A.

Core, section, interval (cm)	Top interval (mbsf)	Bottom interval (mbsf)	Pollen and spores			Dinocysts	Wood/ carbonized particles	Ericson Zone (inferred from forams)	Age (inferred from forams)
			Abundance	Preservation	Major types recorded				
155-941A-									
1H-CC, 20–21	5.29	5.30	f	m	TP, stephanocolpate	b	r	Z	Holocene
2H-CC, 32–33	15.50	15.51	r	p	Euphorbiaceae	b	r	RW (Y)	late Pleist.
5H-CC, 91–92	42.56	42.57	r	p	TC, monolete spore	b	r	RW (Y+X)	late Pleist.
9X-CC, 12–31	74.82	74.83	r	m	Cyperaceae, trilete spore	b	r	RW (Y)	late Pleist.
14X-CC, 14–15	124.07	124.08	b			r	r	RW (Y)	late Pleist.
15X-CC, 27–28	139.45	139.46	b			b	f	Y (?)	late Pleist.
17X-CC, 14–15	156.46	156.47	r	m	Cyatheaceae	b	f	Y (?)	late Pleist.
19X-CC, 27–28	176.84	176.85	b			r	f	Y (?)	late Pleist.

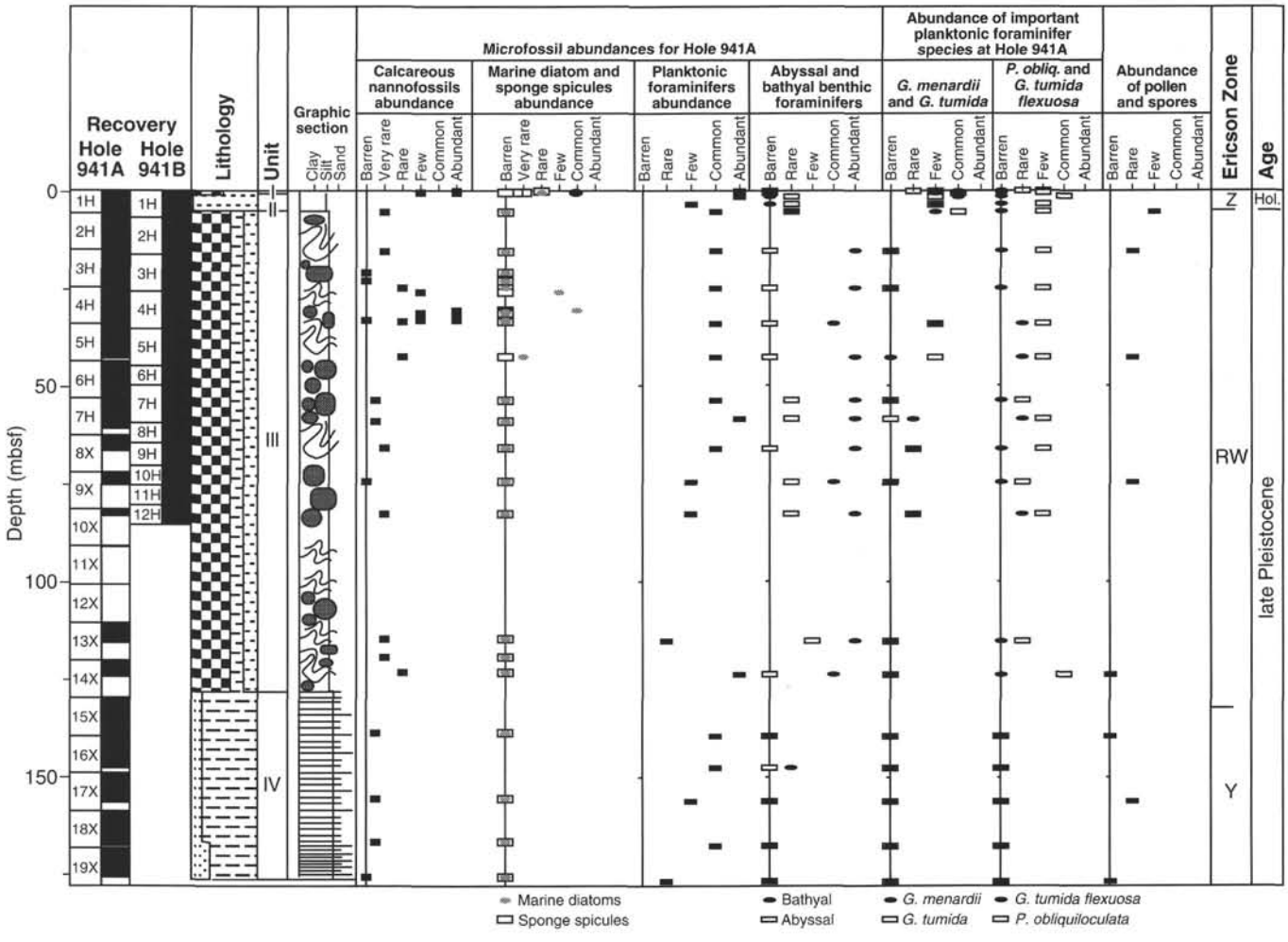

Figure 27. Biostratigraphic summary for Hole 941A.

941A, longitudinal resistivity is approximately 0.44 Ωm, and the rate of downhole decrease is reduced. A change in the downhole trend occurs within Unit IV at 154 mbsf, and from this depth to the base of the hole, resistivity is approximately 0.40 Ωm.

Resistivity anisotropy in Holes 941A and 941B displays high variability in Unit III and slightly more negative values in Unit IV (Fig. 36). The distinction between mass transport and levee deposits on the basis of resistivity anisotropy is not as obvious as at previous Amazon Fan sites. At Site 941, the average anisotropy for the silty clay levee deposits of Unit IV, –2.4%, is only slightly greater than that of the mass transport sediment of Unit III, –1.7%.

CORE-SEISMIC INTEGRATION

Hole 941A was drilled through the Western Debris Flow of the Amazon Fan into an underlying levee (probably the Purple Channel-levee System) of the Upper Levee Complex (Damuth et al., 1983; Manley and Flood, 1988). Three seismic-facies units are identified on 3.5-kHz and on water-gun seismic profiles (*JOIDES Resolution* 0328UTC on 06 May 1994). Seismic-facies Unit 1 is classified using 3.5-kHz profiles (Fig. 3), whereas Units 2 and 3 are classified from the water-gun profiles (Fig. 2).

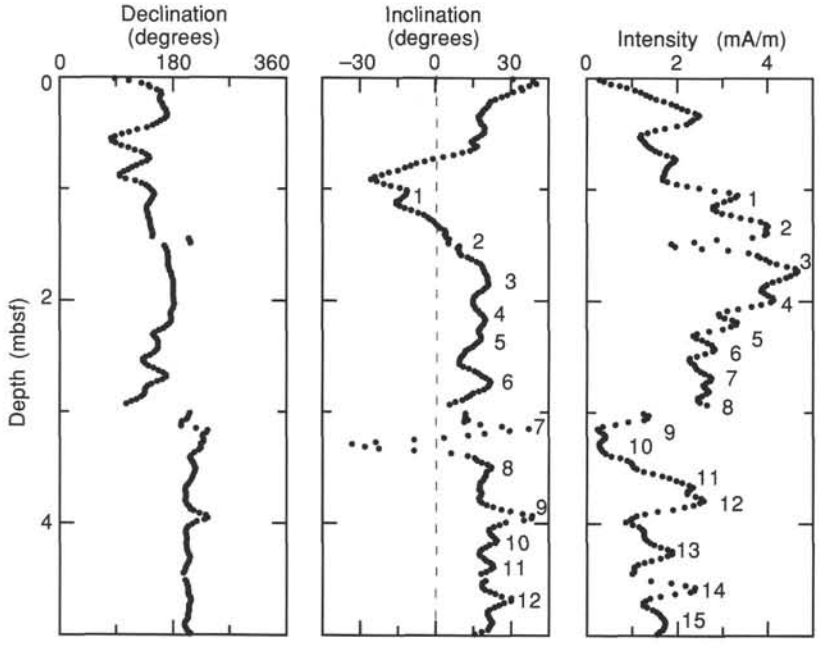

Figure 28. Declinations, inclinations, and remanence intensity, after AF demagnetization to 20 mT, for Core 155-941A-1H. Declination is not corrected azimuthally. Inclination and intensity peaks are numbered sequentially.

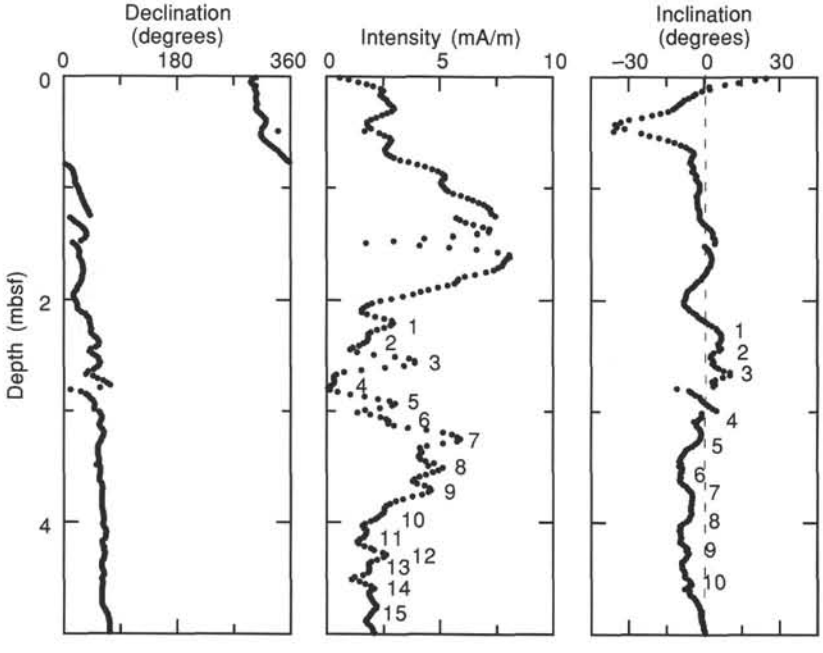

Figure 29. Declinations, inclinations, and remanence intensity, after AF demagnetization to 20 mT, for Core 155-941B-1H. Declination is not corrected azimuthally. Inclination and intensity peaks are numbered sequentially.

Preliminary correlation between the seismic-facies units and the lithologic units (Fig. 37) was made by using the velocity-depth equation determined at Site 931. Seismic-facies Unit 1 (0 to 8 ms) is acoustically transparent and correlates to the hemipelagic Holocene sediment of lithologic Units I and II. Lithologic Unit I is a brown calcareous clay, and Unit II is composed of dark gray silty clay with no silt laminae. Seismic-facies Unit 2 (8–170 ms), distinguished by low-amplitude, hummocky to chaotic reflections, correlates with the inferred debris-flow deposit of lithologic Unit III. Seismic-facies Unit 3 (170–250 ms) exhibits low- to medium-amplitude, discontinuous, subparallel divergent reflections, which are returned from sediment within the buried Purple(?) Channel-levee System. This seismic unit correlates to lithologic Unit IV, which is composed of dark gray silty clay with abundant silt laminae and thin beds, interpreted as levee overbank deposits. The prominent reflection at 170 ms represents the boundary between the base of the Western Debris Flow and the underlying Purple(?) Channel-levee System.

IN-SITU TEMPERATURE MEASUREMENTS

Temperature gradients and heat flow were determined using one downhole measurement and the bottom-water (mud-line) temperature. An ADARA measurement was made during Core 941A-6H (52.8 mbsf) using instrument number 12. The mud-line temperature of 2.6°C measured from this instrument was used as the reference

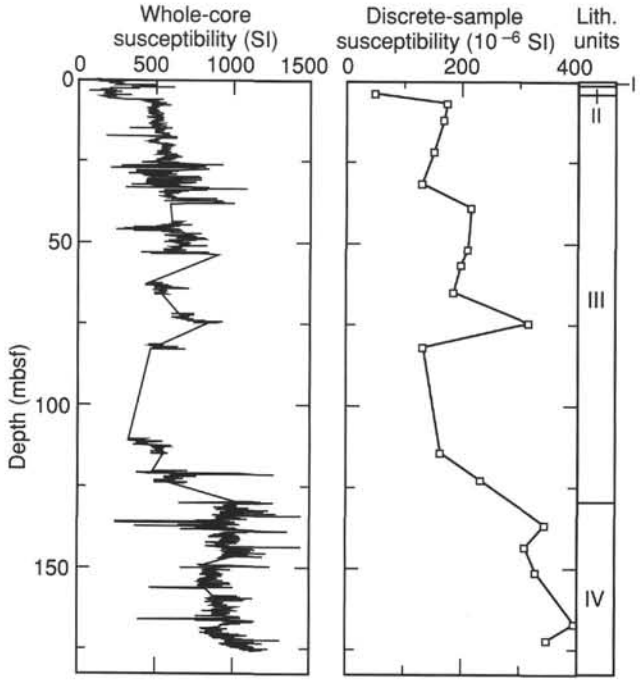

Figure 30. Whole-core and discrete-sample magnetic susceptibility for Site 941.

Table 6. Gas concentrations in sediments from Site 941.

Core, section, interval (cm)	Depth (mbsf)	Sed. temp.* (°C)	Methane HS (ppm)	Methane VAC (ppm)
155-941A-				
1H-2, 0–5	1.50	2	342	
2H-6, 0–5	11.56	2	34,940	
3H-6, 0–5	22.30	3	8,974	
4H-2, 0–5	25.78	3	7,975	453,417
5H-3, 0–5	36.80	3	8,249	295,999
6H-8, 0–5	52.58	4	6,811	60,944
7H-6, 0–5	58.08	4	4,645	
8X-3, 0–5	65.20	4	8,323	
9X-2, 0–5	73.30	4	6,941	
10X-1, 0–5	81.30	5	1,044	
13X-3, 0–5	112.37	6	9,746	
14X-2, 0–5	121.50	6	6,774	
15X-5, 0–5	135.70	6	5,682	
16X-4, 0–5	143.80	7	6,485	
17X-3, 0–5	151.90	7	7,068	
18X-4, 0–5	163.10	7	7,421	
19X-4, 0–5	172.70	8	6,708	

Notes: HS = headspace; VAC = vacutainer. Geothermal gradient = 32°C/km. Bottom-water temperature = 2°C. *See "In-situ Temperature Measurements" section, this chapter.

bottom-seawater temperature at Site 941. A successful measurement resulted in an extrapolated equilibrium temperature of 4.26°C.

The equilibrium temperature, extrapolated from a synthetic curve constructed to fit transient temperature data, is plotted as a function of depth (mbsf) in Figure 38. Using the ADARA mud-line temperature and the sub-bottom temperature from the ADARA measurement downhole, the geothermal temperature gradient can be approximated by a linear mean of 31.6°C/km. We calculated heat flow by adopting the constant geothermal temperature gradient of 31.6°C/km and a linear increase in thermal conductivity, K, of 1.05 ± 0.15 W/(m·K), which is an average of regression estimates at 60 mbsf. This results in a calculated heat flow of 33.21 mW/m^2.

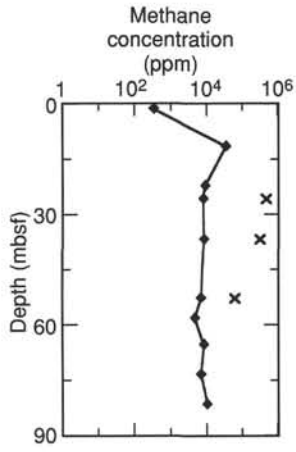

Figure 31. Methane concentrations at Site 941. Headspace (diamond) and vacutainer (×) samples are plotted.

SYNTHESIS AND SIGNIFICANCE

Stratigraphic Synthesis

Surficial Nannofossil-Foraminifer Clay (Unit I)

Unit I (0–0.98 mbsf) is a Holocene bioturbated nannofossil-foraminifer clay (Fig. 39), with about 30% carbonate. Hole 941A is exceptional in that the calcareous clay is underlain by a foraminifer sand (with 80% carbonate) with abundant pteropod shells, interpreted as a turbidite; no iron-rich diagenetic crust is present. This foraminifer sand is absent in Hole 941B, but the iron-rich crust is present.

Lower Holocene Bioturbated Mud (Unit II)

Unit II (0.98–5.30 mbsf) consists of bioturbated, dark gray mud, with carbonate content that decreases downhole from 5.7% to 0.6%. The unit also contains a Holocene foraminiferal fauna including *G. tumida*. Euhedral crystals of ikaite, several centimeters in size, were found at 3–4 mbsf. They began to disintegrate a few hours after the core was split. Paleomagnetic inclination shows 10 to 15 oscillations interpreted to be geomagnetic secular variation between 1 and 5 mbsf in Unit II.

Mass-transport ("Debris-flow") Deposit (Unit III)

Unit III (5.30–129.70 mbsf) consists of mud and sandy mud of varying consistency and color. Soft-sediment deformation, both ductile and brittle, is common. The presence of clasts is indicated by abrupt changes in lithology and color. Folds occur on scales from centimeters to meters. Some boundaries between clasts show ductile shear deformation. Fault contacts are common, and layering in many clasts is offset by sets of microfaults. Rare pebbles of siltstone and unidentified rock are found, but sand is very sparse. In general, the body appears to be a clast-supported breccia, and little matrix mud was identified.

Clasts in the debris-flow deposit are of two main biozones. One type comprises Y zone assemblages including *P. obliquiloculata* (i.e., probably 40–85 ka). The other consists of X zone assemblages including a relatively high abundance of *G. menardii, G. tumida,* and *G. tumida flexuosa,* indicating an interglacial assemblage probably from isotopic Stage 5. Preliminary data suggest that biozones alternate down through the debris-flow deposit, with each zone being 10–20 m thick. In addition, clasts of olive-gray mud with 7% carbonate at 30–35 mbsf contain a rich Miocene nannoflora. Echinoid plates are

Table 7. Elemental and organic carbon compositions of sediments from Site 941.

Core, section, interval (cm)	Depth (mbsf)	IC (%)	$CaCO_3$* (%)	TC (%)	TOC (%)	TN (%)	TS (%)	[C/N]a
155-941A-								
1H-1, 18–19	0.18	3.83	31.9	4.09	0.26	0.07	0.00	4
1H-1, 53–54	0.53	9.51	79.2	9.56	0.04	0.02	0.00	3
1H-2, 25–26	1.75	0.23	1.9	0.94	0.71	0.07	0.07	12
1H-3, 29–30	3.29	0.69	5.7	1.32	0.63	0.07	1.99	10
1H-3, 124–125	4.24	0.07	0.6	0.69	0.62	0.06	1.41	11
2H-3, 100–101	8.06	0.26	2.2	1.01	0.75	0.08	0.23	12
2H-4, 32–33	8.88	0.33	2.7	1.05	0.72	0.08	0.15	10
2H-5, 100–101	11.06	0.32	2.7	1.16	0.84	0.08	0.11	12
3H-3, 43–44	18.23	0.27	2.2	1.09	0.82	0.08	0.18	11
4H-5, 92–93	31.16	0.82	6.8	1.42	0.60	0.09	0.13	8
5H-3, 60–61	37.40	0.31	2.6	1.09	0.78	0.08	0.12	12
6H-2, 98–99	44.56	0.26	2.2	0.98	0.72	0.09	0.14	10
6H-6, 138–139	50.96	0.29	2.4	1.02	0.73	0.08	0.13	11
7H-4, 59–60	55.67	0.34	2.8	0.99	0.65	0.09	0.15	9
7H-5, 109–110	57.67	0.32	2.7	1.04	0.72	0.09	0.29	9
8X-2, 69–70	64.39	0.33	2.7	1.03	0.70	0.09	0.30	9
9X-1, 53–54	72.33	0.29	2.4	0.91	0.62	0.08	0.22	9
10X-1, 54–55	81.84	0.49	4.1	1.15	0.66	0.10	0.22	8
13X-2, 59–60	111.46	0.28	2.3	0.96	0.68	0.09	0.74	9
13X-3, 120–121	113.57	0.37	3.1	1.05	0.68	0.08	0.18	9
14X-1, 16–17	120.16	0.62	5.2	1.24	0.62	0.08	0.26	9
14X-3, 16–17	123.16	0.33	2.7	1.04	0.71	0.09	0.21	9
15X-1, 7–8	129.77	0.33	2.7	1.04	0.71	0.08	0.13	11
16X-3, 92–93	143.22	0.29	2.4	1.11	0.82	0.09	0.07	11
16X-5, 71–72	146.01	0.33	2.7	1.20	0.87	0.11	0.09	9
17X-5, 7–8	154.97	0.36	3.0	1.19	0.83	0.10	0.09	10
17X-5, 10–11	155.00	0.33	2.7	0.62	0.29	0.06	0.12	6
18X-4, 62–63	163.72	0.29	2.4	0.90	0.61	0.07	0.20	10
18X-4, 65–66	163.75	0.43	3.6	1.25	0.82	0.10	0.19	10
19X-5, 62–63	174.82	0.30	2.5	1.09	0.79	0.08	0.10	11
19X-5, 64–65	174.84	0.14	1.2	0.54	0.40	0.05	0.09	10

Note: * = calculated assuming all IC is calcite.

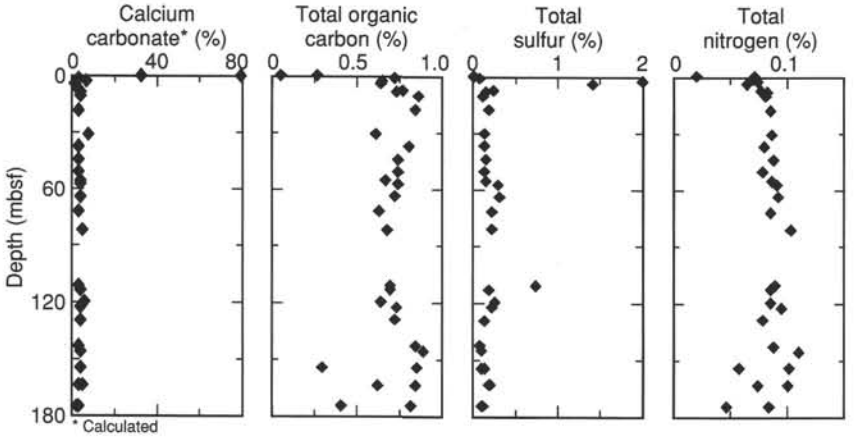

Figure 32. Concentration profiles of calcium carbonate, total organic carbon, total sulfur, and total nitrogen in Hole 941A.

Table 8. Interstitial water chemistry, Site 941.

Core, section, interval (cm)	Depth (mbsf)	Salinity	pH	Alkalinity (mM)	Cl^- (mM)	Mg^{2+} (mM)	Ca^{2+} (mM)	K^+ (mM)	HPO_4^{2-} (μM)	SO_4^{2-} (mM)	NH_4^+ (mM)	H_4SiO_4 (μM)	Na^+ (mM)	Fe^{2+} (μM)	Mn^{2+} (μM)
155-941A-															
1H-2, 145–150	2.95	34.0	8.11	14.51	552	43.1	6.4	12.2	198.9	11.3	1.1	138	477	11.2	2.8
2H-6, 150–155	13.06	32.0	7.65	11.87	554	37.7	4.5	9.1	10.4	0.3	4.6	285	469	34.3	3.2
3H-5, 145–150	22.25	32.0	7.50	11.00	558	39.9	5.0	9.3	10.9	0.3	5.8	294	464	99.5	4.4
4H-5, 145–150	31.69	32.0	7.68	12.43	563	37.7	4.6	9.1	26.0	0.3	6.8	281	475	23.2	8.0
5H-2, 143–150	36.72	32.0	7.55	10.18	563	38.5	4.8	13.0	13.0	0.5	6.8	357	468	62.9	4.0
8X-2, 140–150	65.10	32.0	7.29	9.22	544	38.8	5.4	7.1	8.7	2.5	8.5	355	454	77.0	3.6
13X-2, 140–150	112.27	29.5	7.57	8.64	496	29.5	4.2	6.1	2.9	0.5	7.3	287	425	11.4	2.8
16X-4, 140–150	145.20	33.0	7.09	9.00	556	41.2	5.4	6.3	0.5	0.5	6.5	376	460	23.2	4.8
19X-3, 140–150	173.60	33.0	7.62	10.59	566	43.5	5.6	6.6	9.8	3.1	7.9	298	470	86.4	4.4

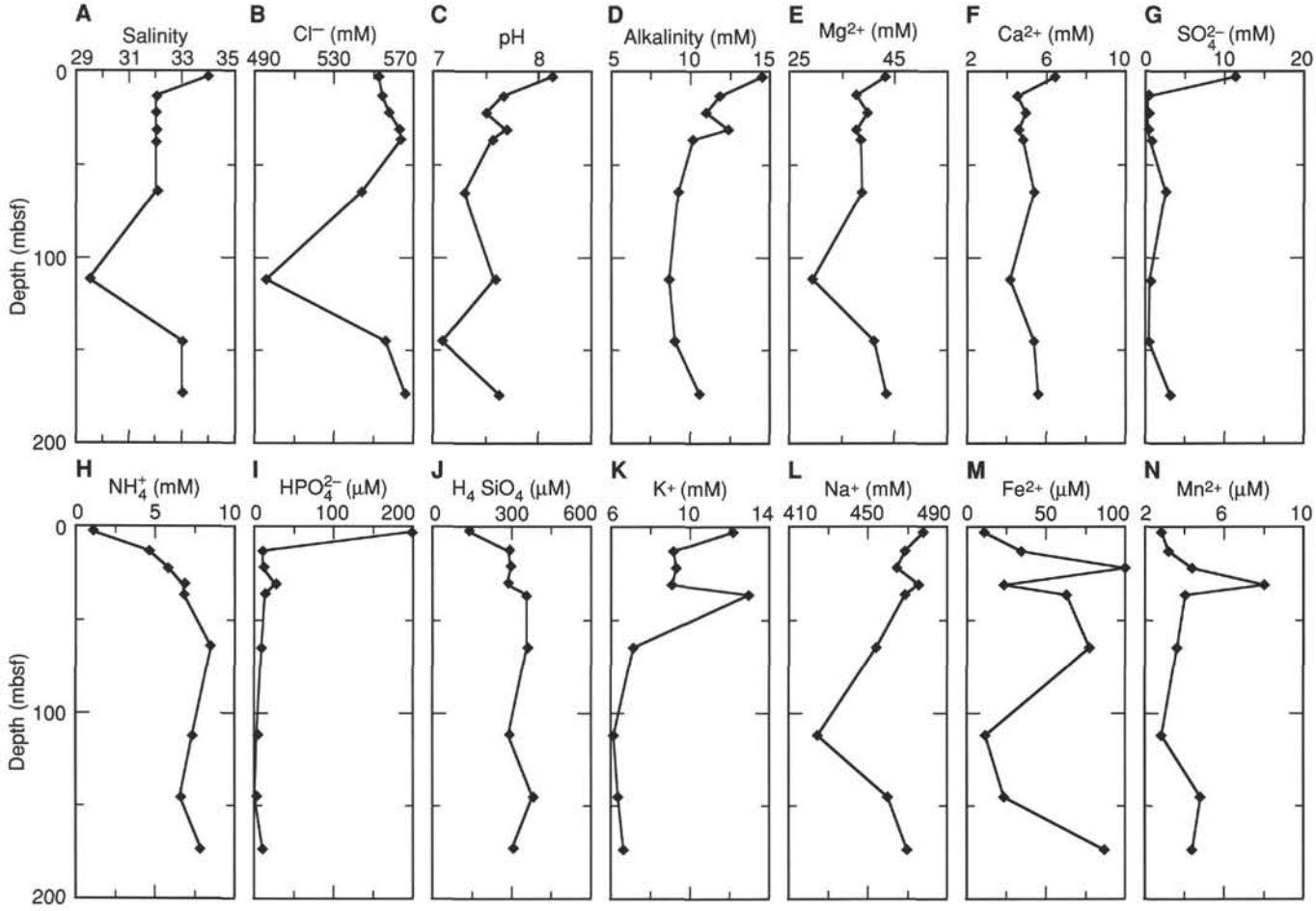

Figure 33. Downhole variation in pore-water chemistry. **A.** Salinity. **B.** Chloride. **C.** pH. **D.** Alkalinity. **E.** Magnesium. **F.** Calcium. **G.** Sulfate. **H.** Ammonium. **I.** Phosphate. **J.** Silica. **K.** Potassium. **L.** Sodium. **M.** Iron. **N.** Manganese.

locally abundant. Bathyal benthic foraminifers, pteropods, ostracod shells, and fish scales are also found in Unit III.

Unit III is interpreted as a debris-flow or slump deposit, but the number of depositional events is uncertain. Recovery was very poor in the lower half of this unit (24% from 72 to 130 mbsf).

Levee Flank of the ?Purple Levee System (Unit IV)

Unit IV (129.70–177.90 mbsf) consists of mud with many laminae and thin beds of silt and fine sand, similar to levee sequences cored at other sites of Leg 155. The unit contains a Y-zone fauna lacking *P. obliquiloculata* and is therefore interpreted as younger than 40 ka. This age supports the suggestion that the levee correlates with the Purple Channel-levee System that was cored at Site 930.

Implications

This site provided a detailed section through a young debris-flow deposit, with a total volume of about 2000 km^3, which appears to be of earliest Holocene age. Similar mass-transport deposits cover about 40% of the present fan surface above 4000 m water depth. Previous seismic-reflection profiles on the Amazon Fan, confirmed by Leg 155 holes, have shown that about 20% of the sediment in the upper few hundred meters of the middle and upper fan is made up of a few vast debris-flow deposits of the type cored at this site.

Unit III shows many of the sedimentological features that could only be inferred in the more deeply buried debris-flow deposits recovered by XCB drilling. The general lack of muddy matrix material is noteworthy. Blocks are inferred to range in size from centimeters to many meters and are both folded and faulted. The repetitive biozones suggest that the debris-flow deposit may have formed by repeated retrogressive failure of a stratigraphic section comprising glacial-age sediment overlying last-interglacial sediment. The 500-m offset between the two holes has shown no evidence for correlation of individual blocks between holes. Nevertheless, the correlation of the repetitive biozones indicates some lateral continuity in the deposit.

The debris-flow deposit at Site 941 has a relatively flat top in seismic-reflection profiles and fills depressions in topography, unlike debris flows at previous sites (Sites 931, 933, 935, and 936), which tend to have rough tops and drape over pre-existing topography.

Total organic carbon is lower than at other Leg 155 sites, and is typically 0.6%–0.85%. Nevertheless, measured headspace methane concentrations are similar to those at other sites. Debris-flow deposits cored at previous sites (e.g., Sites 931, 933, 935, 936) usually have relatively low and scattered organic carbon values. They also tend to have some pore-water sulfate and some anomalous pore-water chloride concentrations. A possible explanation for the low organic carbon and anomalous pore water is that slumping permits reoxygenation of the sediment, resulting in oxidation of both organic matter and sulfides.

Unlike previous Sites 931, 933, 935, and 936, where deeply buried debris-flow deposits were cored, there is no decrease in wet-bulk density and increase in porosity in the levee sediment immediately

Table 9. Major element composition (wt%) of sediment samples, Site 941.

Core, section, interval (cm)	Depth (mbsf)	Lithology	SiO_2	TiO_2	Al_2O_3	Fe_2O_3	MnO	MgO	CaO	Na_2O	K_2O	P_2O_5	Total	LOI
155-941A-														
3H-3, 46–50	18.26	Mud	59.32	0.94	23.25	8.40	0.07	2.23	0.88	1.45	3.29	0.20	100.03	8.34
8X-2, 71–76	64.41	Mud	60.13	0.95	22.87	8.27	0.08	2.10	0.89	1.46	3.17	0.21	100.11	8.17
13X-3, 121–126	113.58	Mud	61.18	0.93	22.16	7.97	0.10	2.16	0.80	1.54	3.22	0.18	100.25	7.87
16X-5, 72–77	146.02	Mud	61.91	1.04	21.60	7.75	0.11	2.14	0.76	1.43	3.10	0.18	100.03	7.84

Notes: Total iron is reported as Fe_2O_3. LOI = loss on ignition.

Table 10. Trace element composition (ppm) of sediment samples, Site 941.

Core, section, interval (cm)	Depth (mbsf)	Lithology	Ba	Ce	Cr	Cu	Nb	Ni	Rb	Sr	V	Y	Zn	Zr
155-941A-														
3H-3, 46–50	18.26	Mud	492	114	70	35	19	35	147	156	95	33	129	182
8X-2, 71–76	64.41	Mud	478	105	69	34	20	37	141	154	100	33	127	191
13X-3, 121–126	113.58	Mud	473	107	67	33	19	34	140	154	95	35	123	188
16X-5, 72–77	146.02	Mud	502	98	65	36	22	34	136	148	87	38	125	225

underlying the debris-flow deposit, nor is there evidence for overpressuring.

Pore-water phosphate concentration is highest at 3 mbsf. A pore-water sample at 112 mbsf has a salinity of 29.5 and unusually low chloride (496 mM) and magnesium (29.5 mM). These low concentrations suggest pore-water dilution, probably through melting of gas hydrates. The extreme gas expansion and honeycomb structure at 45 mbsf may also be evidence of gas hydrates.

REFERENCES*

Damuth, J.E., 1977. Late Quaternary sedimentation in the western equatorial Atlantic. *Geol. Soc. Am. Bull.*, 88:695–710.

Damuth, J.E., and Embley, R.W., 1981. Mass-transport processes on the Amazon Cone: western equatorial Atlantic. *AAPG Bull.*, 65:629–643.

Damuth, J.E., Flood, R.D., Kowsmann, R.O., Belderson, R.H., and Gorini, M.A., 1988. Anatomy and growth pattern of Amazon deep-sea fan as revealed by long-range side-scan sonar (GLORIA) and high-resolution seismic studies. *AAPG Bull.*, 72:885–911.

Damuth, J.E., Kowsmann, R.O., Flood, R.D., Belderson, R.H., and Gorini, M.A., 1983. Age relationships of distributary channels on Amazon deep-sea fan: implications for fan growth pattern. *Geology*, 11:470–473.

Manley, P.L., and Flood, R.D., 1988. Cyclic sediment deposition within Amazon deep-sea fan. *AAPG Bull.*, 72:912–925.

*Abbreviations for names of organizations and publications in ODP reference lists follow the style given in *Chemical Abstracts Service Source Index* (published by American Chemical Society).

Ms 155IR-117

NOTE: For all sites drilled, core-description forms ("barrel sheets") and core photographs can be found in Section 4, beginning on page 703. Forms containing smear-slide data can be found in Section 5, beginning on page 1199. GRAPE, index property, magnetic susceptibility, and natural gamma data are presented on CD-ROM (back pocket).

Table 11. Index properties at Site 941.

Core, section, interval (cm)	Depth (mbsf)	Water content (%)	Wet-bulk density (g/cm^3)	Grain density (g/cm^3)	Dry-bulk density (g/cm^3)	Porosity (%)	Void ratio
155-941A-							
1H-1, 114–116	1.14	60.9	1.39	2.78	0.54	80.9	4.23
1H-2, 99–101	2.49	44.8	1.60	2.79	0.89	68.8	2.20
1H-3, 110–112	4.10	51.7	1.51	2.82	0.73	74.7	2.95
1H-4, 40–42	4.90	52.6	1.50	2.74	0.71	74.8	2.96
2H-2, 19–21	5.75	40.2	1.65	2.74	0.99	64.2	1.79
2H-2, 104–106	6.60	36.7	1.75	2.82	1.11	61.4	1.59
2H-3, 85–87	7.91	40.4	1.67	2.72	0.99	64.3	1.80
2H-4, 53–55	9.09	39.1	1.71	2.70	1.04	62.9	1.69
2H-5, 74–76	10.80	37.5	1.76	2.78	1.10	62.0	1.63
2H-6, 54–56	12.10	35.4	1.79	2.84	1.16	60.2	1.51
2H-7, 96–98	14.07	33.4	1.80	2.76	1.20	57.4	1.35
2H-8, 37–39	14.98	34.4	1.78	2.72	1.17	58.2	1.39
3H-1, 130–132	16.10	37.6	1.71	2.70	1.06	61.3	1.59
3H-2, 121–123	17.51	30.4	1.86	2.77	1.30	54.1	1.18
3H-3, 78–80	18.58	36.9	1.73	2.81	1.09	61.6	1.60
3H-4, 78–80	20.08	36.2	1.75	2.77	1.12	60.6	1.54
3H-5, 85–87	21.65	35.6	1.75	2.71	1.13	59.3	1.46
3H-6, 90–92	23.20	33.6	1.77	2.72	1.18	57.4	1.35
3H-7, 66–68	24.46	34.0	1.77	2.70	1.17	57.7	1.36
4H-1, 79–81	25.09	35.4	1.78	2.81	1.15	60.1	1.51
4H-2, 74–76	26.52	31.4	1.82	2.72	1.25	54.8	1.21
4H-3, 53–55	27.81	33.2	1.82	2.75	1.22	57.2	1.34
4H-4, 73–75	29.51	32.7	1.84	2.80	1.24	57.0	1.33
4H-4, 104–106	29.82	29.3	1.89	2.75	1.34	52.6	1.11
4H-5, 84–86	31.08	34.7	1.79	2.76	1.17	58.9	1.43
4H-6, 47–49	32.21	35.3	1.77	2.70	1.14	59.0	1.44
4H-7, 45–47	33.69	29.3	1.86	2.71	1.32	52.3	1.10
5H-1, 122–124	35.02	31.5	1.83	2.75	1.25	55.2	1.23
5H-2, 94–96	36.24	30.4	1.87	2.76	1.30	54.0	1.18
5H-3, 95–97	37.75	30.3	1.85	2.79	1.29	54.2	1.18
5H-4, 36–38	38.56	30.2	1.85	2.74	1.29	53.6	1.15
5H-6, 13–15	41.33	30.5	1.84	2.71	1.28	53.8	1.16
6H-2, 102–104	44.60	31.8	1.81	2.73	1.24	55.4	1.24
6H-3, 99–101	46.07	31.7	1.82	2.73	1.24	55.3	1.24
6H-4, 89–91	47.47	31.3	1.88	2.78	1.29	55.3	1.24
6H-5, 108–110	49.16	31.1	1.86	2.81	1.28	55.3	1.24
6H-6, 95–97	50.53	29.6	1.88	2.82	1.33	53.6	1.15
6H-7, 105–107	52.13	29.9	1.89	2.80	1.33	53.8	1.17
6H-8, 73–75	53.31	27.7	1.91	2.77	1.38	51.0	1.04
7H-1, 62–64	53.42	29.1	1.88	2.74	1.33	52.4	1.10
7H-3, 24–26	54.32	27.3	1.91	2.73	1.39	50.0	1.00
7H-4, 13–15	55.21	28.4	1.90	2.78	1.36	51.8	1.08
7H-5, 65–67	57.23	29.6	1.86	2.75	1.31	53.0	1.13
7H-6, 11–13	58.19	28.0	1.92	2.78	1.38	51.3	1.05
8X-1, 85–87	63.15	31.3	1.82	2.70	1.25	54.7	1.21
8X-1, 126–128	63.56	27.9	1.91	2.76	1.38	51.1	1.04
8X-2, 51–53	64.21	28.5	1.88	2.74	1.35	51.6	1.07
8X-3, 34–36	65.54	27.3	1.93	2.77	1.40	50.4	1.02
8X-1, 94–96	72.74	26.1	1.93	2.72	1.42	48.5	0.94
8X-1, 140–142	73.20	27.4	1.93	2.79	1.40	50.7	1.03
8X-2, 22–24	73.52	25.5	2.00	2.81	1.49	48.4	0.94
10X-1, 116–118	82.46	26.9	1.93	2.81	1.41	50.2	1.01
13X-1, 37–39	110.67	30.3	1.85	2.72	1.29	53.5	1.15
13X-2, 62–64	111.49	30.6	1.87	2.80	1.30	54.6	1.20
13X-3, 17–19	112.54	26.8	1.96	2.78	1.43	49.9	1.00
13X-4, 84–86	114.71	27.4	1.95	2.77	1.42	50.5	1.02
14X-1, 41–43	120.41	22.9	2.02	2.74	1.56	44.3	0.79
14X-1, 89–91	120.89	26.4	1.94	2.73	1.43	48.9	0.96
14X-2, 118–120	122.68	24.9	1.99	2.74	1.49	47.0	0.89
14X-3, 6–8	123.06	26.8	1.95	2.73	1.42	49.4	0.98
15X-1, 56–58	130.26	27.8	1.92	2.80	1.39	51.3	1.05
15X-1, 129–131	130.99	27.5	1.91	2.73	1.39	50.3	1.01
15X-2, 37–39	131.57	28.0	1.94	2.77	1.39	51.3	1.05
15X-3, 98–100	133.68	27.8	1.94	2.78	1.40	51.1	1.04
15X-4, 41–43	134.61	28.0	1.91	2.71	1.37	50.8	1.03
15X-5, 81–83	136.51	27.9	1.92	2.78	1.38	51.2	1.05
15X-6, 68–70	137.88	27.8	1.91	2.75	1.38	50.8	1.03
15X-7, 30–32	139.00	25.3	1.98	2.74	1.48	47.6	0.91
16X-1, 67–69	139.97	27.2	1.92	2.72	1.39	49.8	0.99
16X-2, 132–134	142.12	28.2	1.92	2.79	1.38	51.7	1.07
16X-3, 100–102	143.30	28.5	1.92	2.79	1.37	52.0	1.08
16X-4, 35–37	144.15	26.8	1.96	2.77	1.43	49.7	0.99
16X-5, 48–50	145.78	26.1	1.97	2.77	1.45	48.9	0.96
16X-6, 10–12	146.90	27.3	1.93	2.77	1.40	50.4	1.02
17X-1, 72–74	149.62	28.8	1.91	2.78	1.36	52.3	1.10
17X-2, 73–75	151.13	29.0	1.89	2.71	1.34	51.9	1.08
17X-3, 52–54	152.42	28.3	1.93	2.77	1.38	51.6	1.07
17X-4, 65–67	154.05	29.0	1.91	2.74	1.36	52.3	1.10
17X-5, 62–64	155.52	28.2	1.92	2.75	1.38	51.3	1.06
18X-1, 61–63	159.21	26.9	1.95	2.73	1.42	49.5	0.98
18X-2, 95–97	161.05	27.6	1.96	2.78	1.42	50.9	1.04
18X-3, 86–88	162.46	26.3	1.96	2.71	1.45	48.6	0.95
18X-4, 98–100	164.08	26.7	1.97	2.74	1.45	49.3	0.97
18X-5, 66–68	165.26	25.8	2.02	2.76	1.50	48.3	0.94
18X-6, 112–114	167.22	26.0	1.98	2.79	1.47	48.8	0.95
19X-1, 104–106	169.24	27.0	1.94	2.71	1.42	49.4	0.98
19X-2, 110–112	170.80	27.0	1.93	2.74	1.41	49.7	0.99

Table 11 (continued).

Core, section, interval (cm)	Depth (mbsf)	Water content (%)	Wet-bulk density (g/cm^3)	Grain density (g/cm^3)	Dry-bulk density (g/cm^3)	Porosity (%)	Void ratio
19X-3, 67–69	171.87	27.2	1.94	2.80	1.41	50.5	1.02
19X-4, 83–85	173.53	26.3	1.94	2.72	1.43	48.7	0.95
19X-5, 70–72	174.90	25.8	1.99	2.76	1.48	48.3	0.94
155-941B-							
1H-2, 72–74	2.22	52.1	1.50	2.82	0.72	74.93	2.99
1H-4, 72–74	5.22	55.4	1.44	2.69	0.64	76.58	3.27
2H-2, 79–81	8.89	36.3	1.75	2.77	1.11	60.66	1.54
2H-4, 66–68	11.76	37.6	1.73	2.81	1.08	62.29	1.65
2H-5, 96–98	13.56	36.2	1.77	2.80	1.13	60.79	1.55
2H-7, 16–18	15.76	36.2	1.74	2.76	1.11	60.40	1.53
3H-5, 36–38	20.54	33.1	1.79	2.75	1.20	56.99	1.32
3H-6, 26–28	21.15	33.9	1.80	2.80	1.19	58.38	1.40
3H-6, 123–125	22.12	35.1	1.75	2.72	1.13	58.93	1.43
3H-7, 3–5	22.42	35.0	1.79	2.77	1.16	59.21	1.45
3H-7, 128–130	23.67	34.5	1.78	2.75	1.17	58.58	1.41
3H-CC, 6–8	24.52	34.1	1.79	2.71	1.18	57.79	1.37
4H-2, 97–99	26.90	32.2	1.83	2.77	1.25	56.19	1.28
4H-3, 102–104	28.45	32.6	1.83	2.79	1.23	56.80	1.31
4H-4, 37–39	29.30	32.5	1.86	2.81	1.25	56.89	1.32
4H-5, 76–78	30.21	32.7	1.83	2.80	1.23	57.01	1.33
4H-6, 109–111	31.97	31.5	1.84	2.75	1.26	55.24	1.23
4H-7, 74–76	33.12	32.2	1.83	2.77	1.24	56.16	1.28
5H-2, 85–87	37.45	31.7	1.84	2.76	1.26	55.53	1.25
5H-3, 67–69	38.77			2.78			
5H-4, 29–31	39.26	32.3	1.84	2.80	1.25	56.58	1.30
5H-5, 80–82	40.41	31.8	1.85	2.78	1.26	55.86	1.27
5H-6, 106–108	42.17	31.7	1.85	2.74	1.27	55.35	1.24
6H-3, 74–76	48.34	36.4	1.74	2.73	1.11	60.40	1.53
7H-1, 42–44	50.02	30.8	1.84	2.74	1.28	54.37	1.19
7H-3, 54–56	53.14	31.1	1.84	2.73	1.27	54.60	1.20
7H-4, 62–64	54.72	29.8	1.88	2.72	1.32	52.92	1.12
7H-5, 17–19	55.77	25.3	1.99	2.72	1.48	47.35	0.90
7H-5, 119–121	56.79	25.8	2.01	2.79	1.49	48.67	0.95
7H-6, 6–8	57.16	24.8	1.98	2.74	1.49	46.80	0.88
7H-6, 142–144	58.52	28.9	1.88	2.75	1.34	52.12	1.09
7H-CC, 4–6	59.01	28.6	1.92	2.81	1.37	52.31	1.10
8H-2, 54–56	61.03	28.1	1.91	2.76	1.38	51.31	1.05
8H-3, 99–01	62.28	26.9	1.95	2.82	1.43	50.32	1.01
8H-4, 5–7	62.84	25.1	2.00	2.74	1.50	47.26	0.90
8H-5, 120–22	64.35	25.7	1.99	2.80	1.48	48.58	0.94
9H-1, 66–8	64.76	26.2	1.94	2.73	1.43	48.60	0.95
9H-2, 131–133	66.91	27.1	1.93	2.73	1.41	49.75	0.99
9H-3, 114–116	68.24	29.3	1.90	2.72	1.34	52.39	1.10
9H-4, 5–7	68.65	29.2	1.90	2.75	1.34	52.47	1.10
10H-2, 118–120	72.06	28.9	1.93	2.79	1.38	52.52	1.11
10H-3, 20–22	72.58	28.7	1.89	2.72	1.35	51.58	1.07
10H-4, 55–57	74.43	29.2	1.92	2.84	1.36	53.34	1.14
11H-1, 31–33	75.41	33.4	1.81	2.73	1.20	57.21	1.34
11H-2, 49–51	77.09	29.7	1.89	2.79	1.33	53.48	1.15
11H-3, 84–86	78.15	28.5	1.92	2.74	1.37	51.66	1.07
11H-4, 31–33	78.98	29.3	1.91	2.72	1.35	52.44	1.10
11H-5, 89–91	80.10	28.0	1.93	2.72	1.39	50.80	1.03
12H-3, 120–122	83.13	26.9	1.93	2.72	1.41	49.41	0.98
12H-4, 8–10	83.51	26.3	1.97	2.72	1.45	48.65	0.95
12H-4, 86–88	84.29	27.5	1.93	2.74	1.40	50.39	1.02

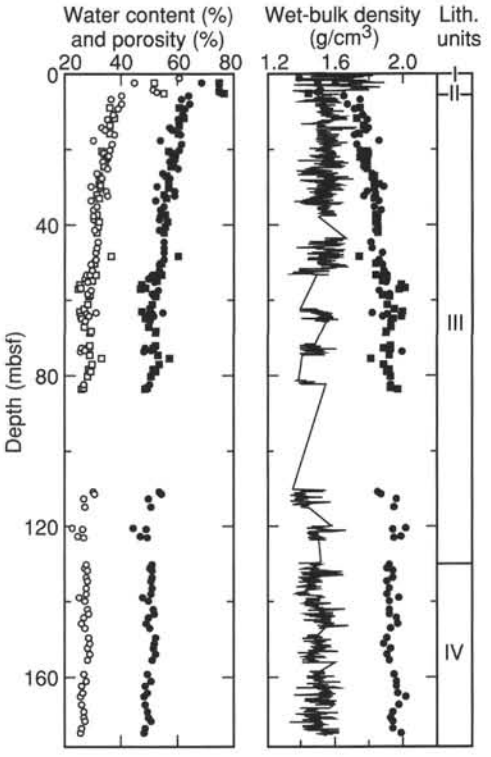

Figure 34. Water content (open symbols) and porosity (solid symbols) for Holes 941A (circles) and 941B (squares); wet-bulk density as determined for discrete samples for Holes 941A (circles) and 941B (squares) and by the GRAPE for Hole 941A (line).

Table 12. Undrained shear strength at Site 941.

Core, section, interval (cm)	Depth (mbsf)	Peak undrained shear strength (kPa)	Residual undrained shear strength (kPa)	Unconfined compressive strength* (kPa)
155-941A-				
1H-1, 115	1.15	4.6	3.4	
1H-2, 100	2.50	3.8	2.9	
1H-3, 111	4.11	4.3	3.0	
1H-4, 41	4.91	5.0	3.6	
2H-2, 20	5.76	11.6	8.5	
2H-2, 105	6.61	11.6	8.7	
2H-3, 86	7.92	5.7	4.1	
2H-4, 54	9.10	7.9	5.4	
2H-5, 75	10.81	9.3	6.1	
2H-6, 55	12.11	35.9	18.9	
2H-7, 97	14.08	17.8	12.2	
2H-8, 38	14.99	32.0	19.8	
3H-1, 131	16.11	11.7	8.2	
3H-2, 122	17.52	44.3	21.9	
3H-3, 79	18.59	8.0	5.6	
3H-4, 79	20.09	13.9	10.6	
3H-5, 86	21.66	21.8	15.1	
3H-6, 91	23.21	25.5	15.6	
3H-7, 67	24.47	26.0	17.7	
4H-1, 80	25.10	23.5	15.4	
4H-2, 75	26.53	19.0	13.7	
4H-3, 54	27.82	26.3	14.0	
4H-4, 74	29.52	36.2	22.2	
4H-4, 105	29.83	95.9	81.2	
4H-4, 109	29.87	30.3	19.3	
4H-5, 85	31.09	29.1	15.9	
4H-6, 48	32.22	23.8	13.4	
4H-7, 46	33.70	31.1	20.0	
5H-1, 123	35.03	37.3	21.3	
5H-2, 97	36.27	36.5	21.4	
5H-3, 96	37.76	34.2	21.9	
5H-4, 37	38.57	39.3	23.4	
5H-6, 14	41.34	37.6	23.0	
6H-2, 103	44.61	31.4	19.6	73.6
6H-3, 100	46.08	42.2	22.5	93.2
6H-4, 90	47.48	51.8	24.7	127.5
6H-5, 109	49.17	52.9	26.2	107.9
6H-6, 96	50.54	55.5	30.4	103.0
6H-7, 106	52.14	46.3	25.9	112.8
6H-8, 73	53.31	55.0	31.4	137.3
7H-1, 63	53.43	65.8	37.6	147.2
7H-3, 25	54.33	63.8	29.2	171.7
7H-4, 13	55.21	76.1	42.2	176.6
7H-5, 67	57.25	50.9	30.2	117.7
7H-6, 12	58.20	54.0	30.7	137.3
8X-1, 85	63.15	15.9	12.0	73.6
8X-1, 126	63.56	35.5	23.6	107.9
8X-2, 52	64.22	47.3	28.2	122.6
8X-3, 35	65.55	31.4	17.6	157.0
9X-1, 94	72.74	44.7	26.5	137.3
9X-1, 140	73.20	44.2	26.9	132.4
9X-2, 25	73.55	53.5	33.0	196.2
10X-1, 117	82.47	38.6	24.9	127.5
13X-1, 39	110.69	31.9	20.8	112.8
13X-2, 63	111.50	36.0	20.6	112.8
13X-3, 18	112.55			157.0
13X-4, 84	114.71	54.5	31.8	181.5
14X-1, 36	120.36	58.3	40.3	201.1
14X-1, 90	120.90	42.4	30.0	171.7
14X-2, 117	122.67	69.8	46.6	235.4
14X-3, 7	123.07	61.9	36.5	137.3
15X-1, 55	130.25	50.4	28.7	117.7
15X-1, 130	131.00	35.4	25.9	93.2
15X-2, 38	131.58	51.3	33.9	137.3
15X-3, 98	133.50	40.7	28.1	98.1
15X-4, 41	134.61	51.3	33.7	127.5
15X-5, 82	136.50			88.3
15X-6, 69	137.89	39.8	26.7	107.9
15X-7, 31	139.01	66.3	33.0	176.6
16X-1, 66	139.96	52.2	33.7	122.6
16X-2, 133	142.13	36.2	24.7	127.5
16X-3, 100	143.30	27.4	19.0	117.7
16X-4, 36	144.16	31.8	22.2	103.0
16X-5, 49	145.79	77.8	47.8	171.7
16X-6, 13	146.93	78.7	43.8	171.7
17X-1, 74	149.64	45.1	31.4	117.7
17X-2, 73	151.13	59.2	37.0	132.4
17X-3, 53	152.43	65.4	40.9	117.7
17X-4, 66	154.06	38.9	27.3	122.6
17X-5, 63	155.53	44.2	29.8	117.7
18X-1, 62	159.22	65.4	38.6	132.4
18X-2, 96	161.06	73.4	33.9	157.0
18X-3, 87	162.47	76.9	39.9	176.6
18X-4, 99	164.09	90.2	50.2	171.7
18X-5, 67	165.27	85.8	45.3	161.9
18X-6, 113	167.23	101.7	47.7	201.1
19X-1, 105	169.25	52.2	35.9	
19X-2, 111	170.81	65.4	39.1	157.0
19X-3, 68	171.88	63.6	41.8	147.2
19X-4, 84	173.54	53.9	35.5	127.5
19X-5, 71	174.91	67.2	42.6	157.0
155-941B-				
1H-2, 72	2.22	5.7	4.6	
1H-4, 73	5.23	6.2	4.9	
2H-2, 80	8.90	15.0	10.4	
2H-4, 66	11.76	10.7	7.7	
2H-5, 97	13.57	14.7	11.1	
2H-7, 16	15.76	16.7	12.2	
3H-5, 37	20.55	22.6	15.2	
3H-6, 27	21.16	22.9	15.2	
3H-6, 124	22.13	22.1	15.4	
3H-7, 4	22.43	17.8	12.3	
3H-7, 129	23.68	16.1	12.1	
3H-CC, 6	24.52	20.4	14.0	
4H-2, 98	26.91	30.3	19.0	
4H-3, 103	28.46	33.7	20.9	
4H-4, 38	29.31	33.4	18.5	
4H-5, 77	30.22	45.5	24.7	
4H-6, 110	31.98	43.3	25.7	
4H-7, 75	33.13	51.4	28.5	
5H-2, 90	37.50	30.9	21.1	
5H-3, 68	38.78	32.4	20.4	
5H-4, 30	39.27	35.5	19.8	
5H-5, 81	40.42	33.9	22.1	
5H-6, 107	42.18	36.5	23.4	
6H-3, 75	48.35	9.8	6.6	
7H-1, 43	50.03	22.1	14.7	
7H-3, 55	53.15	31.9	22.6	
7H-4, 63	54.73	43.2	28.0	117.7
7H-5, 18	55.78	59.1	35.5	107.9
7H-5, 120	56.80	68.1	38.1	181.5
7H-6, 7	57.17	61.9	36.8	132.4
7H-6, 143	58.53	60.1	34.2	127.5
7H-CC, 5	59.02	66.3	36.3	117.7
8H-2, 59	61.08	52.2	35.1	112.8
8H-3, 100	62.29	61.0	32.7	132.4
8H-4, 6	62.85	78.7	40.9	157.0
8H-5, 121	64.36	78.7	44.2	142.3
9H-1, 67	64.77	74.3	43.9	171.7
9H-2, 132	66.92	80.4	48.1	196.2
9H-3, 115	68.25	75.1	34.9	196.2
9H-4, 6	68.66	83.1	39.1	196.2
10H-2, 119	72.07	117.6	64.1	220.7
10H-3, 21	72.59	145.0	74.0	294.3
10H-4, 56	74.44	97.2	55.7	196.2
11H-1, 32	75.42	58.3	30.5	117.7
11H-2, 50	77.10	86.6	43.0	181.5
11H-3, 85	78.16	132.6	66.3	245.3
11H-4, 32	78.99	86.6	38.3	181.5
11H-5, 95	80.16	105.2	56.6	220.7
12H-3, 121	83.14	77.8	46.0	191.3
12H-4, 9	83.52	84.9	47.9	181.5
12H-4, 9	83.52	64.5	40.6	152.1

Note: *Unconfined compressive strength (q_u) can be used to approximate undrained shear strength (S_u) by the relationship $q_u = 2S_u$.

Table 13. Electrical resistivity at Site 941.

Core, section, interval (cm)	Depth (mbsf)	Longitudinal resistivity (Ωm)	Transverse resistivity (Ωm)
155-941A-			
1H-1, 115	1.15	0.250	0.219
1H-2, 100	2.50	0.174	0.197
1H-3, 111	4.11	0.180	0.188
1H-4, 41	4.91	0.191	0.195
2H-2, 20	5.76	0.206	0.190
2H-2, 105	6.61	0.245	0.237
2H-3, 86	7.92	0.224	0.238
2H-4, 54	9.10	0.262	0.232
2H-5, 75	10.81	0.283	0.258
2H-6, 55	12.11	0.282	0.272
2H-7, 97	14.08	0.282	0.276
2H-8, 38	14.99	0.279	0.274
3H-1, 131	16.11	0.231	0.229
3H-2, 122	17.52	0.272	0.273
3H-3, 79	18.59	0.235	0.235
3H-4, 79	20.09	0.244	0.240
3H-5, 86	21.66	0.261	0.251
3H-6, 91	23.21	0.252	0.246
3H-7, 67	24.47	0.252	0.255
4H-1, 80	25.10	0.309	0.277
4H-2, 75	26.53	0.310	0.283
4H-3, 54	27.82	0.291	0.291
4H-4, 74	29.52	0.283	0.277
4H-4, 105	29.83	0.318	0.303
4H-5, 85	31.09	0.298	0.297
4H-6, 48	32.22	0.287	0.311
4H-7, 46	33.70	0.323	0.307
5H-1, 123	35.03	0.318	0.303
5H-2, 97	36.27	0.338	0.354
5H-3, 96	37.76	0.327	0.302
5H-4, 37	38.57	0.305	0.308
5H-6, 14	41.34	0.301	0.322
6H-2, 103	44.61	0.339	0.303
6H-3, 100	46.08	0.291	0.300
6H-4, 90	47.48	0.312	0.316
6H-5, 109	49.17	0.327	0.315
6H-6, 96	50.54	0.332	0.314
6H-7, 106	52.14	0.327	0.340
6H-8, 73	53.31	0.343	0.346
7H-1, 63	53.43	0.350	0.368
7H-3, 25	54.33	0.367	0.408
7H-4, 13	55.21	0.415	0.397
7H-5, 67	57.25	0.341	0.361
7H-6, 12	58.20	0.360	0.362
8X-1, 85	63.15	0.371	0.353
8X-1, 126	63.56	0.387	0.387
8X-2, 52	64.22	0.382	0.358
8X-3, 34	65.54	0.414	0.416
9X-1, 94	72.74	0.408	0.406
9X-1, 140	73.20	0.382	0.379
9X-2, 25	73.55	0.444	0.471
9X-2, 93	74.00	0.431	0.439
10X-1, 117	82.00	0.443	0.420
13X-1, 39	110.69	0.400	0.409
13X-2, 63	111.50	0.390	0.382
13X-3, 18	112.55	0.470	0.414
13X-4, 84	114.71	0.409	0.408
14X-1, 39	120.39	0.456	0.479
14X-1, 90	120.90	0.470	0.472
14X-2, 118	122.68	0.470	0.473
14X-3, 7	123.07	0.410	0.424
15X-1, 55	130.25	0.385	0.399
15X-1, 130	131.00	0.395	0.414
15X-2, 38	131.58	0.395	0.386
15X-3, 98	133.68	0.428	0.424
15X-4, 41	134.61	0.460	0.451
15X-5, 81	136.51	0.444	0.429
15X-6, 68	137.88	0.470	0.433
15X-7, 31	139.01	0.498	0.457
16X-1, 66	139.96	0.471	0.468
16X-2, 132	142.12	0.426	0.426
16X-3, 100	143.30	0.415	0.427
16X-4, 36	144.16	0.428	0.462
16X-5, 49	145.79	0.474	0.477
16X-6, 12	146.92	0.480	0.459
17X-1, 73	149.63	0.441	0.447
17X-2, 74	151.14	0.499	0.469
17X-3, 53	152.43	0.437	0.380
17X-4, 66	154.06	0.403	0.417
17X-5, 63	155.53	0.398	0.357
18X-1, 62	159.22	0.398	0.378
18X-2, 89	160.99	0.411	0.388
18X-3, 87	162.47	0.423	0.396
18X-4, 99	164.09	0.418	0.384
18X-5, 67	165.27	0.405	0.393
18X-6, 113	167.23	0.416	0.412
19X-1, 105	169.25	0.374	0.377
19X-2, 111	170.81	0.428	0.407
19X-3, 68	171.88	0.361	0.383
19X-4, 84	173.54	0.391	0.419
19X-5, 71	174.91	0.438	0.383
155-941B-			
1H-2, 72	2.22	0.238	0.236
1H-4, 73	5.23	0.204	0.222
2H-2, 80	8.90	0.323	0.312
2H-4, 65	11.75	0.291	0.280
2H-5, 97	13.57	0.287	0.281
2H-7, 16	15.76	0.301	0.298
3H-5, 37	20.55	0.335	0.330
3H-6, 27	21.16	0.302	0.302
3H-6, 124	22.13	0.327	0.330
3H-7, 4	22.43	0.289	0.304
3H-7, 129	23.68	0.335	0.322
3H-CC, 6	24.52	0.297	0.302
4H-2, 98	26.91	0.317	0.323
4H-3, 103	28.46	0.338	0.295
4H-4, 38	29.31	0.313	0.331
4H-5, 77	30.22	0.320	0.305
4H-6, 110	31.98	0.349	0.376
4H-7, 75	33.13	0.345	0.305
4H-7, 90	33.28	0.362	0.334
5H-2, 86	37.46	0.375	0.351
5H-3, 68	38.78	0.346	0.329
5H-4, 30	39.27	0.323	0.326
5H-5, 81	40.42	0.344	0.361
5H-6, 107	42.18	0.333	0.322
6H-3, 75	48.35	0.302	0.322
7H-1, 43	50.03	0.376	0.362
7H-3, 55	53.15	0.342	0.341
7H-4, 63	54.73	0.372	0.373
7H-5, 18	55.78	0.389	0.373
7H-5, 120	56.80	0.417	0.384
7H-6, 7	57.17	0.380	0.408
7H-6, 143	58.53	0.361	0.348
7H-CC, 5	59.02	0.354	0.368
8H-2, 55	61.04	0.355	0.355
8H-3, 100	62.29	0.393	0.385
8H-4, 6	62.85	0.414	0.378
8H-5, 121	64.36	0.384	0.366
9H-1, 67	64.77	0.446	0.388
9H-2, 132	66.92	0.397	0.386
9H-3, 115	68.25	0.354	0.386
9H-4, 6	68.66	0.411	0.387
10H-2, 119	72.07	0.387	0.395
10H-3, 21	72.59	0.380	0.388
10H-4, 56	74.44	0.381	0.381
11H-1, 32	75.42	0.420	0.333
11H-2, 50	77.10	0.384	0.381
11H-3, 85	78.16	0.390	0.391
11H-4, 32	78.99	0.389	0.372
11H-5, 90	80.11	0.392	0.395
12H-3, 121	83.14	0.382	0.363
12H-4, 9	83.52	0.429	0.422
12H-4, 87	84.30	0.391	0.378

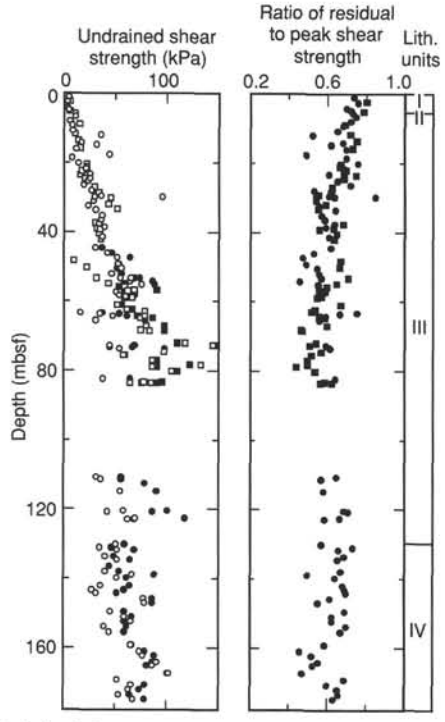

Figure 35. Undrained shear strength (open symbols) and assumed undrained shear strength derived from unconfined compressive strength (solid symbols) in Holes 941A (circles) and 941B (squares); ratio of residual undrained shear strength to peak undrained shear strength for Holes 941A (circles) and 941B (squares).

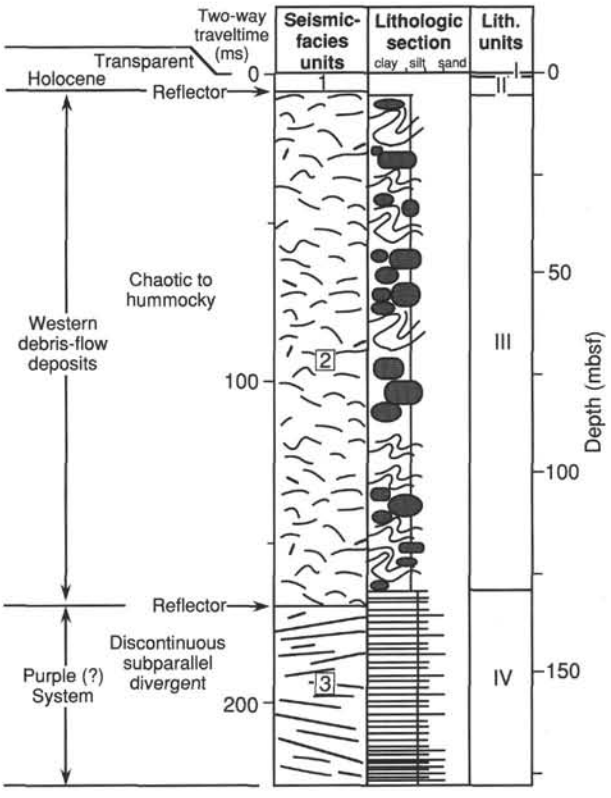

Figure 37. Correlation of lithostratigraphic observations with seismic-facies units and prominent reflections at Site 941.

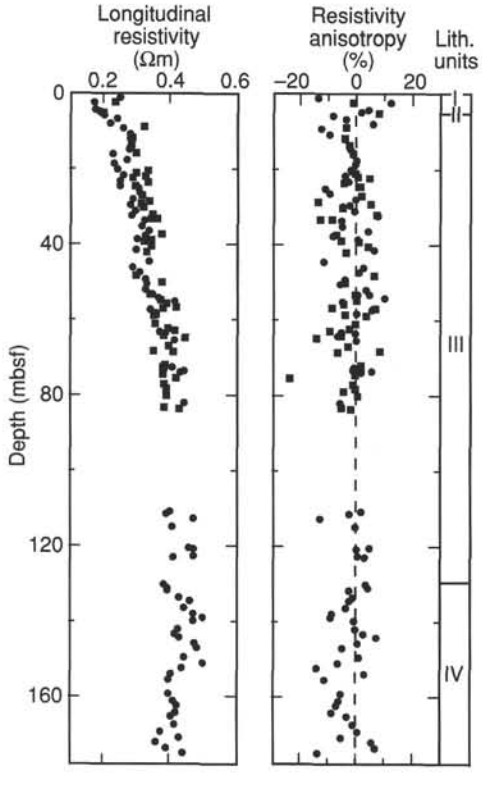

Figure 36. Longitudinal resistivity and resistivity anisotropy in Holes 941A (circles) and 941B (squares).

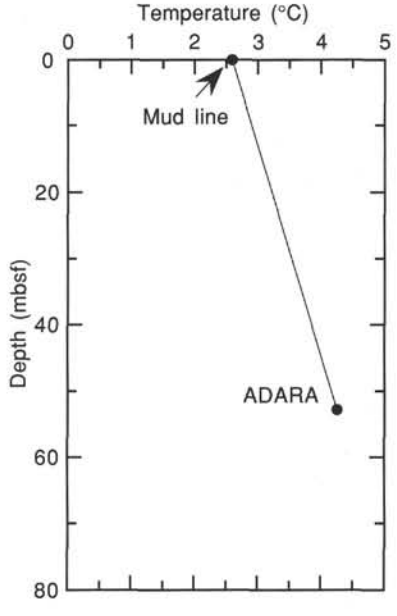

Figure 38. Estimated equilibrium temperatures in Hole 941A. A linear fit indicates a geothermal gradient of 31.6°C/km.

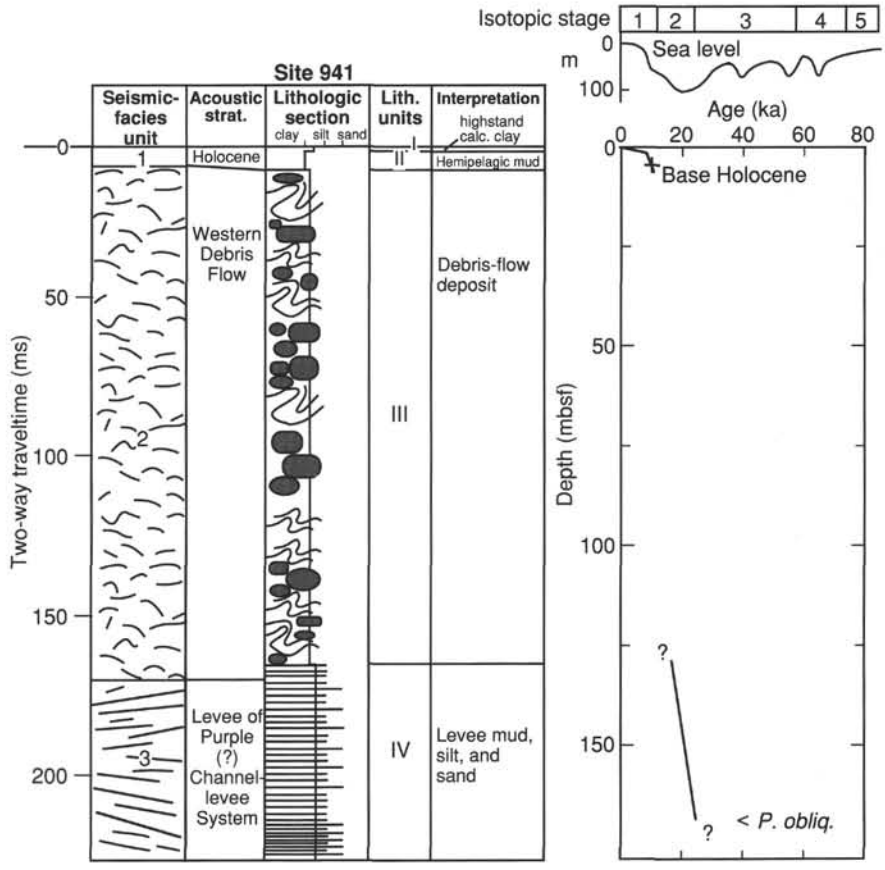

Figure 39. Summary of Site 941 showing (left to right) seismic-facies units, acoustic stratigraphy, schematic lithologic column, lithologic units, interpreted sediment facies, chronological picks, and interpreted age-depth curve (+ = datums; < = younger than a datum; variations in slope between these points are interpreted, based on dated intervals of similar facies at other sites). For explanations of individual columns, see appropriate section of this site chapter.